

**New skeleton and associated skull
of *Homunculus patagonicus* Ameghino, 1891
(Primates, Platyrrhini), from the Miocene of Patagonia (Argentina)**

**Jonathan M.G. Perry, Sergio F. Vizcaíno, M. Susana Bargo, Néstor Toledo,
Kellyn Sanders, Edwin Dickinson, Paul E. Morse, and Richard F. Kay**

ABSTRACT

We describe a new skull and partial skeleton of *Homunculus patagonicus* Ameghino, 1891a, from the Early-Middle Miocene Santa Cruz Formation of Argentinian Patagonia (Santacrucian South American Land Mammal Age, late Early Miocene). All known Santacrucian material fits within a single genus *Homunculus*, and most of the material in a single species: *H. patagonicus*. Full consideration of the cranial and dental specimens collected over the past 20 years (representing several individuals) permits a re-evaluation of the paleobiology of *Homunculus* species. New body mass estimates averaging 2,164 g are produced based on humeral and femoral long-bone cross sections of the new specimen reported here. The new estimate is considered in the context of previous estimates for *Homunculus patagonicus*. Evaluation of the new and previously described postcranial material leads us to infer that *Homunculus* was a generalized arboreal quadruped that used pronograde locomotion with flexed elbow and knee joints, pronated forearms, and occasional leaping through a gap-filled canopy; it likely spent much of its time climbing and clinging to large upright supports. The skull reinforces previous inferences that *Homunculus* ate relatively resistant foods that incorporated or were covered by grit. Based on the new body mass and endocranial volume estimates, we confirm that *Homunculus* had a relatively small brain compared with most extant platyrrhines. The olfactory bulb of *Homunculus* widely overlaps with extant anthropoids in relative size.

Jonathan M.G. Perry. Department of Physical Therapy Education, College of Health Sciences - Northwest, Western University of Health Sciences, 2665 S. Santiam Hwy., Lebanon, Oregon, 97355, U.S.A.
jperry@westernu.edu

Sergio F. Vizcaíno. División Paleontología Vertebrados, Museo de La Plata, Unidades de Investigación Anexo Museo, Av. 60 y 122, B1900FWA, La Plata, Argentina. vizcaino@fcnym.unlp.edu.ar

M. Susana Bargo. División Paleontología Vertebrados, Museo de La Plata, Unidades de Investigación Anexo Museo, Av. 60 y 122, B1900FWA, La Plata, Argentina. msbargo@fcnym.unlp.edu.ar

Final citation: Perry, Jonathan M.G., Vizcaíno, Sergio F., Bargo, M. Susana, Toledo, Néstor, Sanders, Kellyn, Dickinson, Edwin, Morse, Paul E., and Kay, Richard F. 2025. New skeleton and associated skull of *Homunculus patagonicus* Ameghino, 1891 (Primates, Platyrrhini), from the Miocene of Patagonia (Argentina). *Palaeontologia Electronica*, 28(2):a21.
<https://doi.org/10.26879/21>
palaeo-electronica.org/content/2025/5526-new-skeleton-of-fossil-primate-from-miocene-of-argentina

Copyright: May 2025 Society of Vertebrate Paleontology.

This is an open access article distributed under the terms of the Creative Commons Attribution License, which permits unrestricted use, distribution, and reproduction in any medium, provided the original author and source are credited.
creativecommons.org/licenses/by/4.0

Néstor Toledo. División Paleontología Vertebrados, Museo de La Plata, Unidades de Investigación Anexo Museo, Av. 60 y 122, B1900FWA, La Plata, Argentina. ntoledo@fcnym.unlp.edu.ar

Kellyn Sanders. CMI, Medical and Biological Illustrator, Sanders Medical Media, LLC. ksmedicalmedia@gmail.com

Edwin Dickinson. Department of Anthropology and Archaeology, University of Calgary, 2500 University Dr. N.W., Calgary, AB, T2N 1N4, Canada. edwin.dickinson@ucalgary.ca

Paul E. Morse. Department of Cell and Developmental Biology, University of Colorado Anschutz Medical Campus School of Medicine, Aurora, CO 80045, U.S.A. paul.morse@cuanschutz.edu

Richard F. Kay. Departments of Evolutionary Anthropology & Earth and Climate Sciences, Duke University, Durham, NC 27708, U.S.A. Richard.Kay@duke.edu

Keywords: Primates, Santacrucian, Santa Cruz Formation, Pinturas Formation, paleobiology, diet, locomotion, body mass

Submission: 7 October 2024. Acceptance: 10 April 2025.

INTRODUCTION

Primates occur as a rare component of fossil assemblages in the Late Oligocene and Early Miocene of South America. Platyrrhine primates are an important indicator of the presence of forested environments in the fossil record. Their Early-Middle Miocene occurrence in Argentina at latitudes as high as 51°S offers evidence of a far southerly extension of forests during the Miocene Climatic Optimum (Trayler et al., 2020a; Kay et al., 2021), thousands of kilometers south of their current subtropical range between ~20°S and 17°S. The earliest Miocene primates from Argentina are *Tremacebus* at 42.5°S (Hershkovitz, 1974), *Dolichocebus* at 43.2°S (Kraglievich, 1951), and *Mazonicebus* at 45.6°S (Kay, 2010) from the Sarmiento Formation of Chubut Province in the Colhuehuapian South American Land Mammal Age (SALMA) (~21 Ma). *Chilecebus* at ~35°S (Flynn et al., 1995) from the Abanico Formation of Chile is younger than these (~20 Ma). Next to occur in the temporal sequence are *Soriacebus* and *Carlocebus* at 50.5°S (Fleagle et al., 1987; Fleagle, 1990) from the Pinturas Formation of Santa Cruz Province (~18-17 Ma; Perkins et al., 2012). *Homunculus* is represented by more skeletal elements and recorded from more localities (Kay et al., 2012; Kay and Perry, 2019) than any other Miocene platyrrhine. It occurs between ~18 and 16.3 Ma (Cuitiño et al., 2016; Trayler et al., 2020b) and attains the southern-most latitude ever achieved by platyrrhines (or any primate), at 51.6°S. Indeed, the paleolatitude at the time of deposition would have been ~55°S, when continental drift is accounted for, whereas the present latitude of the southern tip of Africa is ~35°S. Almost all specimens belong to *Homunculus pata-*

gonicus Ameghino, 1891a (Perry et al., 2014), and are known from Atlantic coastal exposures of the Santa Cruz Formation (SCF; Santacrucian SALMA; Early-Middle Miocene; Kay et al. 2012). However, another species, *H. vizcainoi*, comes from inland exposures of the SCF along the Río Santa Cruz (Kay and Perry, 2019).

These Early Miocene genera are now considered by most (see e.g., Beck, et al., 2023) to constitute an early radiation of tropical platyrrhines that expanded into high latitudes during warm and wet periods. Phylogenetic analyses indicate that these monkeys went extinct without leaving any descendants and bear no special relationship to extant platyrrhine subclades; that is, they are stem platyrrhines (Kay, 2025; Kay and Fleagle, 2010; Kay et al., 2012). Debate about the platyrrhine fossil record included hypotheses (e.g., Rosenberger, 1979a; Rosenberger, 1982; Rosenberger, et al., 2011) that postulated sister relationships between individual Early Miocene genera to living platyrrhine families and even living genera (e.g., *Dolichocebus* and *Saimiri*). Rigorous examination of the fossils facilitated by micro-CT scanning and phylogenetic analyses have demonstrated that resemblances between Early Miocene and living genera are primitive traits, examples of convergence, or artifacts of preservation (Kay et al., 2004).

Here we offer a preliminary description of a new skeleton of *Homunculus* from the locality Puesto Estancia La Costa (=Corrighuen Aike, see below; Vizcaino et al., 2012). The specimen includes the cranium and mandible, as well as parts of the axial skeleton and fore- and hindlimbs. This material is the first-known example of an Early Miocene platyrrhine to preserve a well-docu-

mented skeletal and dental association, and the only such example in a stem platyrrhine. The only other Miocene platyrrhine skeleton is that of *Cebupithecia sarmentoi*, from the Middle Miocene of Colombia (Meldrum and Fleagle, 1988; Meldrum and Kay, 1990). In this paper, the cranium, mandible, and dentition are described using conventional surface anatomy and micro-CT data. They support the reconstruction of *Homunculus* as an arboreal species with a mixed diet of fruits and leaves that engaged in quadrupedal locomotion with some leaping and climbing on vertical supports.

Historical Context

The first Miocene platyrrhine described was *Homunculus patagonicus* Ameghino, 1891a. In a publication in August of 1891, Florentino Ameghino described the new genus and species based on a fragmentary mandible that his brother Carlos Ameghino had collected in southern Santa Cruz Province, Argentina. Fortunately, the type specimen, although now misplaced, was figured by Ameghino (1891b: figs. 1-4), and later by Bluntschli (1931: fig. 6). W.B. Scott also photographed the specimen; the photo (reproduced here as Figure 1) is in the collections of the Yale Peabody Museum.

Even in his brief initial description, Florentino Ameghino recognized that this primate was lemur-like, but more “elevated” than any early Tertiary primates then known from Europe or North America (Ameghino, 1891a). In October of 1891, Alcides Mercerat (1891) described another primate from the Santa Cruz Formation along the Río Santa Cruz that he named *Ecphantodon ceboides*, based on a mandibular fragment with a single worn tooth. Mercerat made no mention of *Homunculus* in his description, and Ameghino was quick to publish a more extensive description of *Homunculus* before



FIGURE 1. Type specimen of *Homunculus patagonicus*, MACN-A 634. Photograph, taken in 1901 by W.B. Scott. The photograph is housed in the collections of the Yale Peabody Museum, New Haven, Connecticut, U.S.A.

the end of that year (Ameghino, 1891b), along with descriptions of three additional species of primates based on specimens his brother had collected in Santa Cruz Province: *Anthropops perfectus*, *Homocentrus argentinus*, and *Eudiastatus lingulatus*. The first of these has been synonymized with *Homunculus patagonicus*. *Homocentrus* (Bluntschli, 1931, fig. 42) is a rodent, and *Eudiastatus* (Bluntschli, 1931, fig. 43) is a notoungulate. In neither 1891 publication did Ameghino give a precise locality for the specimens; however, he indicated that the specimens were collected on the fourth of his brother Carlos' expeditions (June 1890-June 1891), from between the Río Deseado and the Río Gallegos. In his correspondence with his brother Florentino (10 March 1891), Carlos Ameghino indicated that the holotype had come from the banks of the Río Gallegos (Vizcaíno, 2011), likely from “Felton’s Estancia”, a place now called Killik Aike Norte. Carlos reiterated this information in an interview with Hans Bluntschli in 1911 (Bluntschli, 1913, 1931). Additional specimens described by Florentino (Ameghino, 1898) as *Homunculus patagonicus* were collected by Carlos Ameghino at the coastal locality then known as Corriguen Aike, currently known as Puesto Estancia La Costa (e.g., Tauber, 1991, 1997; Tejedor and Rosenberger, 2008; Kay et al., 2012). These include possibly associated skeletal material: a mandibular fragment (MACN-A 5757, see acronyms section below), a complete right femur (MACN-A 5758), a partial ulna (MACN-A 5759), a complete left radius (MACN-A 5760), and a right distal humeral fragment (MACN-A 5761). A facial fragment (MACN-A 5968), also found by Carlos Ameghino, preserves the left orbit, part of the frontal, and the maxilla, and might (or might not) belong to the same individual (see Table 1 and Kay et al., 2012)

From the time of Ameghino until the late 1900s, no new discoveries of *Homunculus* were reported. Isolated teeth referred to *Homunculus patagonicus* were described from Monte León and Cerro Observatorio, north of the prior record of this species (Fleagle et al., 1988; Fleagle, 1990). Then, in the 1990s, Adán A. Tauber surveyed the coast of Santa Cruz Province and rediscovered many of the productive localities from the early 1900s, as well as new localities (Tauber, 1991, 1994, 1996, 1997, 1997, 1999; Tauber et al., 2004). As part of his geologic and stratigraphic survey, Tauber established a series of faunal levels. He made a large fossil collection and, in the process, discovered and described a partial cranium of *Homunculus*

(CORD-PZ 1130) from Puesto Estancia La Costa (Tauber, 1991).

Since 2003, a joint expedition of the Museo de La Plata (Argentina) and Duke University (U.S.A.) has recovered several new specimens of *Homunculus patagonicus* from the Santa Cruz Formation.

These include several crania that were not found in definite association with any other skeletal elements (Table 1). These come from Puesto Estancia La Costa and Killik Aike Norte (Figure 2).

TABLE 1. All *Homunculus* specimens^a recovered by the MLP-Duke expeditions, 2003 to 2019.

Year of Discovery	Catalog Number ^b	Element	Loc. ^c	Collector	Publications	Figure in Publication
2003	MPM-PV 3504	Partial mandible with Li2, p2-3, Rm1-3	ELC	Jonathan Perry	(Perry et al., 2010; Kay et al., 2012)	figs. 2, 8; figs. 16.10c, 16.11b, c
2004	MPM-PV 3500	Right humerus missing proximal end	PLC	Jonathan Perry	(Kay et al., 2012; Perry et al., 2018; Fleagle et al., 2022)	fig. 16.15; None; figs. 2-10
2004	MPM-PV 3502	Cranium missing left superior part of braincase and left zygomatic arch	KAN	Carlos Luna	(Perry et al., 2010; Kay et al., 2012; This Publication)	figs. 1, 2, 8; figs. 16.2c, 16.3b, 16.4a, 16.8a, b, d, 16.11a; Figure 8
2004	MPM-PV 3501	Cranium missing anterior part of palate; partly distorted	PLC	Jonathan Perry	(Perry et al., 2010; Kay et al., 2012)	figs. 1, 9; fig. 16.2a
2004	MPM-PV 3503	Left half of cranium with associated upper right cheek teeth	PLC	Richard Kay	(Kay et al., 2012)	fig. 16.2b
2007	MPM-PV 3505	Face, palate, and anterior cranial fossae of a subadult (with deciduous premolars)	PLC	Jonathan Perry	(Kay et al., 2012; Perry et al., 2014)	figs. 1, 4-10; figs. 16.2d-h
2010	MPM-PV 3708	Right hemimandible with p2-4, m1-3, and intact condyle	PLC	Juan Carlos Fernicola	(Kay et al., 2012; Kay and Perry, 2019; Li et al., 2020)	fig. 16.12b; fig. 3.3
2011	MPM-PV 4376	Left mandible with m1-m2 and anterior alveoli	RBu	Leonel Acosta and Sergio Vizcaino	(Li et al., 2020)	None
2013	MPM-PV 19426*	Left mandibular fragment with m1	BB	Néstor Toledo	(Kay and Perry, 2019; Li et al., 2020)	figs. 5.1, 6
2014	MPM-PV 19427*	Right mandible with m1-3 (all broken)	SBB	Jackson Spradley	(Kay and Perry, 2019)	None
2014	MPM-PV 19428*	Left mandibular fragment with m1-2	SBB	Laura Chornogubsky	(Kay and Perry, 2019)	fig. 5.2
2015	MPM-PV 17453	Partial skeleton with associated skull	PLC	Sergio Vizcaino	This Publication; Li et al., 2020	Figures 3, 5, 8, 11-14
2017	MPM-PV 17452	Left m3	RBo	Susana Bargo and Sergio Vizcaino	(Kay and Perry, 2019)	figs. 3.4, 5.3

^aFor a list of specimens discovered by others, see Kay et al. (2012).

^bAll specimens are accessioned at the Museo Regional Provincial "Padre Manuel Jesús Molina" (Río Gallegos, Santa Cruz Province, Argentina). Specimens are listed in order of discovery.

^cSee Figure 2 for map of localities. BB, Barrancas Blancas, Río Santa Cruz; ELC, Estancia La Costa; KAN, Killik Aike Norte; PLC, Puesto Estancia La Costa; RBo, Río Bote; RBu, Rincón del Buque; SBB, Segundas Barrancas Blancas, Río Santa Cruz.

Asterisk indicates specimens that belong to *Homunculus vizcainoi*; all others are *H. patagonicus*.

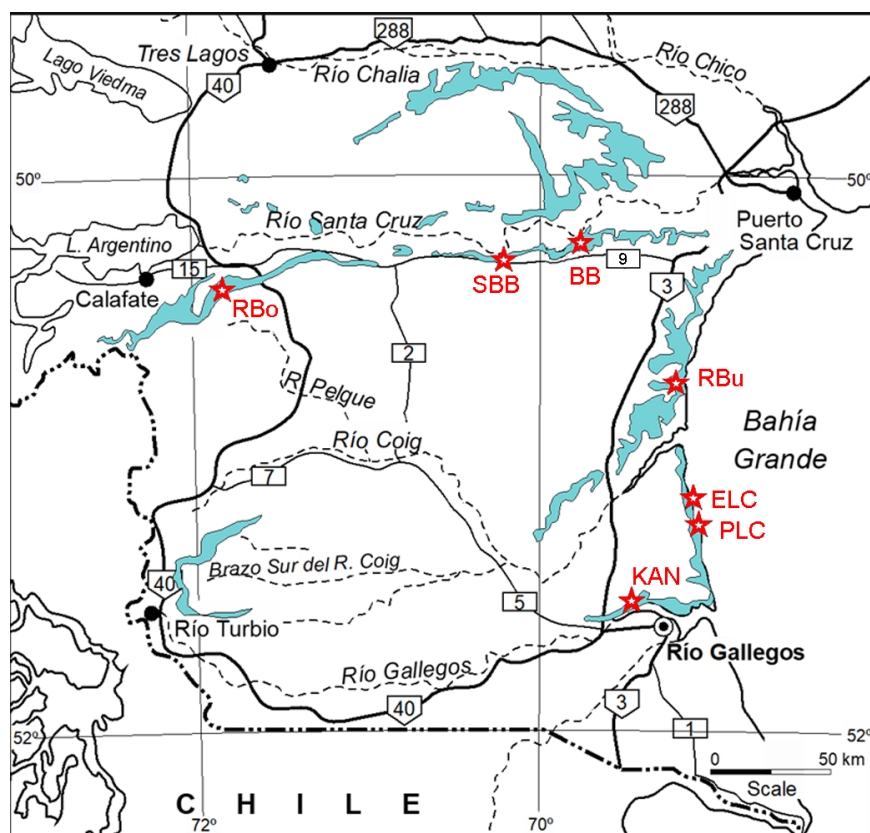


FIGURE 2. Map of southern Patagonia showing principal localities in the text (red stars and text) and in Table 1. Exposures of the Santa Cruz Formation are shown in blue. BB, Barrancas Blancas, Río Santa Cruz; ELC, Estancia La Costa; KAN, Killik Aike Norte; PLC, Puesto Estancia La Costa; RBo, Río Bote; RBu, Rincón del Buque; SBB, Segundas Barrancas Blancas, Río Santa Cruz.

New Discovery and Paleobiological Reconstruction

The present study focuses on a yet undescribed specimen (MPM-PV 17453) recovered in 2015 that includes associated skull and postcranial elements, all excavated in a single block of matrix. This is the first definitively documented associated cranial and postcranial elements of a monkey from the Early-Middle Miocene Santa Cruz Formation of South America, and the first belonging to any stem platyrrhine (e.g., Kay et al., 2004; Kay and Fleagle, 2010; Kay et al., 2012; Kay, 2015). The association of the elements confirms that the previously recorded isolated crania (Perry et al., 2010; Kay et al., 2012; Perry et al., 2014) all belong to *Homunculus patagonicus*. Because the cranium and mandible are of the same individual, we can confirm that the specimens once allocated to a different genus and species (*Killikaika blakei*, based on the rostral part of an isolated cranium, Tejedor et al., 2006) belong to *Homunculus patagonicus*, and can also assess the mechanics of the chewing system

with confidence. The association of skull and limb bones permits us to make and compare body mass estimates from limb dimensions, dental dimensions, and cranial dimensions.

The chewing musculature of *Homunculus patagonicus* has long been considered robust (Tauber, 1991). This is based on its possession of deep muscle scars on the mandible and cranium, indicative of large jaw adductor musculature. Such an inference may well have an influence on paleodietary reconstructions for the animal. Based on additional cranial and mandibular material, Perry et al. (2010) reconstructed jaw adductor muscle leverage and measured tooth root sizes for *Homunculus*. They concluded that muscle leverage (i.e., mechanical advantage) was not especially great relative to extant platyrrhines including capuchins and pitheciines, despite the very large (especially molar) tooth roots and tremendous molar wear. This unique combination of traits for a platyrrhine led to a complex inference of diet: foods were probably somewhat resistant to fracture

requiring heavy loads on the tooth roots; yet, they were probably also very gritty, causing extensive tooth wear. Given the prevalence of volcanism and the likelihood of volcanoclastic soil transportation in its environment (e.g., via dust storms, see Madden, 2015), it is possible that exogenous grit caused much of the extensive tooth wear in *Homunculus*. Perhaps the modest chewing muscle leverage required *Homunculus* to exhibit very large chewing muscles as a compensatory mechanism. One drawback of that study was that none of the crania of *Homunculus* to that point were associated with mandibles, so the chewing model was necessarily a chimera of individuals.

If, as suggested by Perry et al. (2010), the heavy wear on the postcanine teeth of *Homunculus* is due to a diet with copious exogenous grit (rather than inherent food toughness), then this genus was subject to similar environmental pressures attributed to other South American mammals during the Miocene: namely that exogenous grit drove hypsodonty (Madden, 2015). Indeed, because *Homunculus* was likely mainly arboreal, an alternative hypothesis—that hypsodonty in Miocene South American mammals was driven by the spread of grasslands—probably does not apply to this primate.

Li et al. (2020) examined changes in molar sharpness of a wear series of *Homunculus* (including MPM-PV 17453). Based on similar wear modalities of the lower molars between *Homunculus* and *Callicebus*, they concluded that *Homunculus* had a primarily frugivorous diet. However, leaves may have provided an alternative dietary resource to accommodate fluctuation in seasonal fruiting abundance considering it lived in a high-latitude, extratropical environment in late Early Miocene times.

As stated, one problem hampering complete muscle reconstruction for *Homunculus* has been the lack of associated cranial and mandibular material. A second problem has been inadequate sampling of extant platyrrhine chewing muscles and their associated osteological correlates. To confidently reconstruct muscle size, one requires a broad sample of extant analogs with both known muscle dimensions and correlated osteological dimensions (see Perry, 2018). The new specimen of *Homunculus* solves the first problem. The second problem has been solved by studies recently performed on a large and diverse sample of extant platyrrhines (Dickinson et al., 2018; Hartstone-Rose et al., 2018; Deutsch et al., 2020; Dickinson et al., 2022). These studies have quantified fiber

length, muscle mass, and physiological cross-sectional area and compared these data to osteological proxies of soft tissue dimensions, yielding equations that can be used to estimate muscle parameters in fossil platyrrhines.

Several previous estimates of endocranial volume and the size of the olfactory bulbs have been reported in the literature of Early Miocene primates, including for *Homunculus*, *Tremacebus*, and *Chilecebus* (Kay et al., 2012; Ni et al., 2019). Here, we offer new estimates of endocranial volume in MPM-PV 17453 and compare it with new data for the size of these structures in extant anthropoids.

MATERIALS AND METHODS

Acronyms: **CGM**, Cairo Geological Museum, Cairo, Egypt; **CORD-PZ**, Museo de Paleontología, Universidad Nacional de Córdoba, Córdoba, Argentina; **DPC**, Duke Lemur Center Division of Fossil Primates, Durham, North Carolina, U.S.A.; **MACN**, Museo Argentino de Ciencias Naturales “B. Rivadavia”, Colección Nacional Ameghino, Buenos Aires, Argentina; **MLP-PV**, Museo de La Plata Paleontología Vertebrados, La Plata, Argentina; **MPM-PV**, Museo Regional Provincial “Padre M. J. Molina” Paleontología Vertebrados, Río Gallegos, Argentina; **RC**, Rusconi Collection, Museo de Fundación Miguel Lillo, Tucumán, Argentina.

All primate specimens recovered by the MLP-Duke expeditions to date are listed in Table 1.

Field Recovery and CT Scanning

Specimen MPM-PV 17453 was discovered by one of the authors (SFV) during the 2015 field season from fossil horizon 5.3 (Fleagle et al., 2012; Matheos and Raigemborn, 2012; Perkins et al., 2012) at the Puesto Estancia La Costa locality (S51°11'50.8", W069°05'08.9"). The site is approximately 50 m from a subadult partial cranium discovered in 2007 (MPM-PV 3505; S51°11'49.2", W069°05'10.1"), 60 m from an adult cranium found in 2004 (MPM-PV 3501; S51°11'52.1", W069°05'11.3"), and 60 m from another adult cranium found in 2004 (MPM-PV 3503; S51°11'52.4", W069°05'11.7").

MPM-PV 17453 was excavated in such a way as to include all the visible fossil material and subsequent preparation revealed a partial skeleton (Figure 3). The surrounding ground was examined thoroughly to make sure no elements were missed and repeated yearly visits to the locality have not revealed any additional parts. The entire block was CT scanned in a private lab in La Plata using a

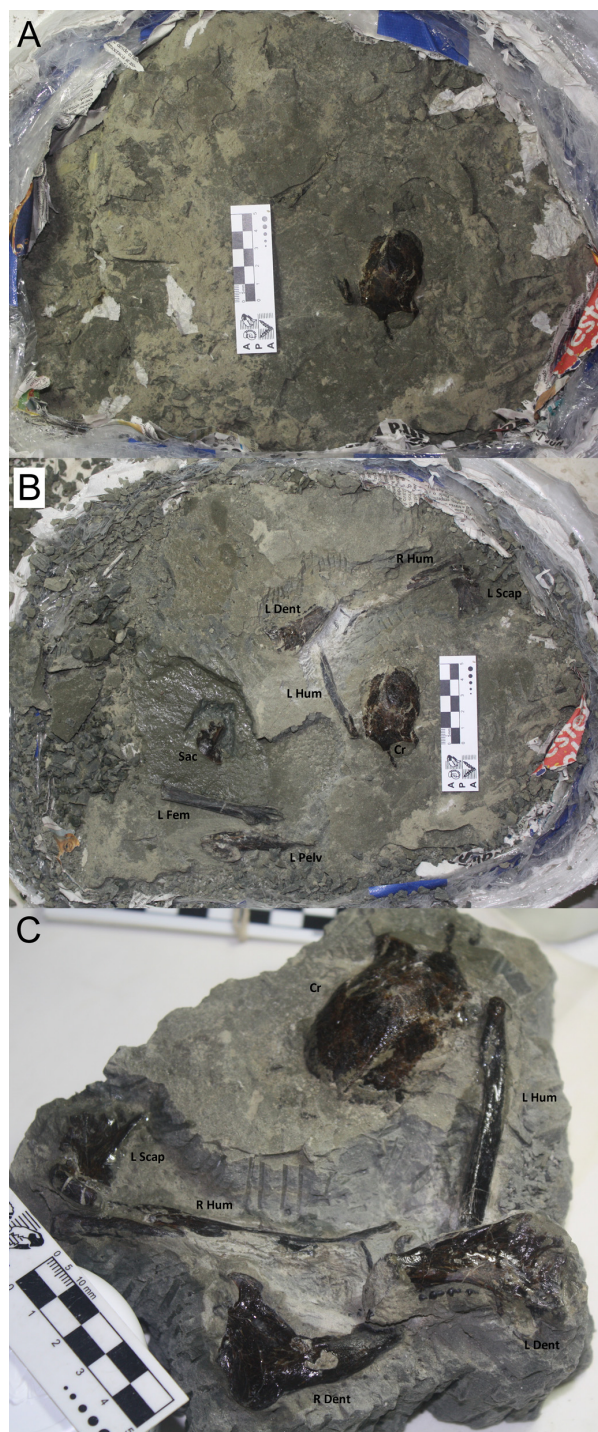


FIGURE 3. Progressive preparation of *Homunculus patagonicus* MPM-PV 17453 showing exposure of skeletal elements. Cr: cranium, Dent: dentary, Fem: femur, Hum: humerus, L: left, Pelv: pelvic bone, R: right, Sac: sacrum, Scap: scapula. **A**, **B**, and **C** are successive stages of preparation.

medical CT scanner. This yielded scans that enabled us to determine which elements were present and that guided subsequent manual preparation at the Museo de La Plata. After preparation was completed, high-resolution scans of various elements were performed in the Y-TEC laboratory (owned jointly by Yacimientos Petrolíferos Fiscales and Consejo Nacional de Investigaciones Científicas y Técnicas) in La Plata, Argentina on a Sky-Scan 1173 micro-CT scanner. Scan parameters were: 130 kV source voltage, 61 μ A source current, 70-micron cubic voxel size.

The specimen belongs to a single individual consisting of a nearly complete cranium with a full adult dentition lacking only the zygomatic arches, with a nearly complete mandible containing all its teeth except the left i1. The mandible is broken asymmetrically at the symphysis. There is a complete right humerus, a left humerus that lacks the proximal end, and two partial scapulae each including the glenoid fossa but missing most of the blades. A left femur lacking the distal end, a partial left pelvic bone, and a partial sacrum are present. All postcranial growth plates are fully fused, and the adult dentition has fully erupted with moderate to heavy wear. Therefore, this specimen is a fully adult individual. The elements were within a few centimeters of one another, and no bones of other animals were recovered in the immediate vicinity.

The completeness of MPM-PV 17453 permits a better understanding of skeletal allometry in *Homunculus* and permits biomechanical analyses of four joints hitherto unavailable from a single individual. These are: 1) the temporomandibular joint (bilaterally), 2) the glenohumeral joint (bilaterally), 3) the hip joint (left side), and 4) the sacroiliac joint (left side).

Analysis

CT-generated scans of individual limb and skull elements were segmented in Avizo (version 8.0, Thermo Fisher Scientific), and these were used to generate scale figures of the skeletal elements. Surface files were printed at natural scale on a Form 3B (Formlabs) 3D printer to assist with measurement and basic anatomical description. To create a virtual brain endocast, 3D segmentation was undertaken by PEM with Avizo3D (Thermo Fisher Scientific). The CT-scans (as a tiff stack) and a 3D model of the MPM-PV 17453 endocast (as a ply file) are available at morphosource.com. Measurements were taken using calipers on the actual specimen (orbit diameter, cranium length), or from surface models at natural scale within

TABLE 2. Prediction variables for *Homunculus* chewing muscle PCSA and mass.

Soft Tissue Variable	Osteological Proxy
Temporalis PCSA	Temporalis Insertion Area, measured from surface of mandible (TIA) Temporalis Origin Area, measured from surface of cranium (TOA)
Masseter PCSA	Masseter Insertion Area, measured from surface of mandible (MIA) Masseter Origin Area, measured from surface of cranium (MOA)
Medial Pterygoid PCSA	Medial Pterygoid Insertion Area, measured from surface of mandible (MPIA) Medial Pterygoid Origin Area, measured from surface of cranium (MPOA)
Temporalis Mass	$TIA \times To-i^a$
Masseter Mass	$MIA \times Mo-i$
Medial Pterygoid Mass	$MPIA \times MPo-i$

^aTo-i is the distance between the centroid of the area of origin to the centroid of the area of insertion for the temporalis. This is measured the same way for Mo-i (masseter) and MPo-i (medial pterygoid).

Avizo (endocast volume, olfactory bulb volume, etc.).

Several other crania of *Homunculus patagonicus* from Santa Cruz Province, Argentina, collected by a joint Museo de La Plata and Duke University team in 2004 (Table 1; Kay et al., 2012; Vizcaíno et al., 2012) were scanned at the University of Texas (UT) at Austin following the same protocols as those described above, and constitute a source of comparative data for the description of MPM-PV 17453 (available on Morphosource). Virtual endocasts were extracted from two of these scans.

Comparative material used for the description also includes *Tremacebus harringtoni*, Colhuehuapian SALMA (~20 Ma). The cranium (RC 619 but referred to by Rusconi as RC 661) is the type specimen of *Tremacebus harringtoni* (Rusconi, 1933; Kay et al., 2004a, fig. 1), which comes from approximately 12 km southwest of Cerro Sacanana, in north central Chubut Province, Argentina. The cranium was scanned at the High-Resolution X-Ray Computed Tomography Facility at UT Austin. Beam energies were set to 150 kV and 160 μ A. The image field was reconstructed to 43 mm, based on a maximum field of view of 44.164 mm, yielding an interpixel spacing of 42 μ m.

Another comparative specimen is that of *Dolichocebus gaimanensis*, Colhuehuapian SALMA (~20 Ma). The cranium of *Dolichocebus gaimanensis* (MACN 14128 from the Trelew Member of the Sarmiento Formation near Gaiman, Chubut Province, Argentina) bears signs of heavy postmortem damage and distortion (Bordas, 1942; Kraglievich, 1951; Rosenberger, 1979a; Hershkovitz, 1982; Rosenberger, 1982; Fleagle and Rosenberger, 1983; Kay et al., 2008). The specimen was scanned at the High-Resolution X-Ray Computed Tomography Facility at UT-Austin using the same

protocol as described above for *Tremacebus*. Slice thickness and interslice spacing was 0.0466 mm (one video line). The image field was reconstructed to 43.5 mm, based on a maximum field of view of 44.164 mm, yielding an interpixel spacing of 42 μ m.

For comparative purposes, we also evaluated the virtual endocasts of the stem catarrhine *Aegyptopithecus zeuxis* (CGM 85785) created and described by Simons et al. (2007), and the stem anthropoid *Simonsius grangeri* (DPC 18651), created and described by Bush and colleagues (Bush et al., 2003, 2004).

Reconstruction of Chewing Muscles

New extant platyrrhine data were used to generate prediction lines for *Homunculus* chewing muscles (E. Dickinson, unpublished data). Muscle physiological cross-sectional area (PCSA) was reconstructed to provide additional data for paleodietary reconstruction (see Perry et al., 2015a; Perry, 2018). Muscle mass estimation was used to provide enhanced accuracy and realism to an artistic life-restoration of *Homunculus* (see below). However, because fiber length is difficult to reconstruct reliably, muscle mass relative to PCSA can be a signal of fiber length and excursion. Both muscle mass and muscle PCSA were estimated using least-squares regressions of extant platyrrhine muscle mass (or PCSA) against related osteological proxies in the same individuals (Table 2). The most reliable proxies of PCSA (for masseter, temporalis, medial pterygoid) are the insertion areas of these muscles as determined by comparing the r-squared values in reduced major axis regressions of the muscle dimension against other available bony proxies used (see Perry, 2018). No good bony proxies for medial pterygoid mass were

found ($r^2 < 0.3$), so an average of the proportion of medial pterygoid mass to temporalis mass, and medial pterygoid mass to masseter mass (from the extant sample) was used to estimate medial pterygoid mass in *Homunculus*.

Before a full reconstruction of the chewing muscles in *Homunculus* could be performed, extensive digital manipulation of the skull was required. This process is described in detail in Sanders (2020). In brief, scanned CT image stacks were viewed in Dragonfly 4.1 (Object Research Systems) and converted to an object file. The remaining sediment matrix adhering to the specimen was then removed digitally (by hand) in Cinema 4D R20 (C4D); any holes created by this process were then patched. The resulting object was then restored in ZBrush 2019 (Maxon Computer GMBH). This consisted of reorienting and sliding fragments of bone into alignment. To achieve the greatest possible realism, a complete skull of *Pithecia pithecia* was used as a reference. This was not because of any special similarity between the extant and extinct species, but only due to the similarity in size and overall shape. Additional specimens of *Homunculus patagonicus* (MPM-PV 3501, MPM-PV 3502, and MPM-PV 3503) were also used for reference. In some instances, parts of *Homunculus patagonicus* cranium MPM-PV 3502 were used to fill in gaps where MPM-PV 17453 is incomplete (e.g., zygomatic arches). Through this process, it was discovered that the right side of the cranium of MPM-PV 17453 is too distorted to permit realistic restoration. Therefore, the left side of the cranium was mirrored in ZBrush; the distorted right hemi-cranium was then replaced with the mirrored left hemi-cranium. Finally, any remaining holes in the model were filled using Blender software (Blender Institute, B.V.).

Next the mandible was aligned and articulated with the cranium. The right half of the mandible is more complete than the left, so the right was mirrored and used to fill in any gaps on the left (including an incisor). Rough edges (including at the symphysis) were smoothed together. The mandible was shifted into articulation with the cranium, leaving a small space between each mandibular condyle and its glenoid fossa to account for an articular disk (thickness estimated to be 2 mm, based on approximate size in extant platyrrhines).

The process for reconstructing the chewing muscles onto the restored skull of MPM-PV 17453 is described in detail in Sanders (2020). The first step in generating anatomically realistic chewing

muscles is to map out the areas of origin and insertion onto the skull. This process was carried out collaboratively between JMGP and KS, drawing on previously published dissections of extant platyrrhine chewing muscles. This process included dissection and observation of a reference extant platyrrhine specimen (*Leontopithecus rosalia*). Muscle attachment maps were drawn onto and anchored to the “undistorted” skull model in ZBrush. Muscle volumes were then created and manipulated using the MoveTopological tool in ZBrush. After every manipulation, the volume of the muscle mesh was checked against the numbers provided by the prediction equations (see below). Then each muscle mesh was provided with a texture to show fiber direction and painted in a color to represent muscle. The whole model was then decimated to reduce the data burden on computing systems and processing time.

Body Mass Estimation

Several previous estimates of body size have been attempted for *Homunculus* based on various isolated cranial, dental, and postcranial elements (see summary by Perry et al., 2018). The association of cranial and postcranial elements in MPM-PV 17453 permits a means of body mass estimation previously unavailable for this or any other Early Miocene platyrrhine. Pampush et al. (2021) assessed the accuracy of primate body mass predictions using various techniques against an extant dataset that included a phylogeny of 24 strepsirrhines, 3 tarsiers, and 20 platyrrhines with *Tupaia* and *Galeopterus* serving as outgroups. They found that phylogenetic independent contrasts (PIC; Garland and Ives, 2000) and BayesModelS (Nunn and Zhu, 2014) have substantially higher predictive accuracy than do ordinary least squares or phylogenetic generalized least squares, regardless of body size proxy. Among the various proxies commonly used in body mass estimation, their most accurate results were obtained from humeral and femoral cross-sections while the most problematic were predictions from dental dimensions.

To estimate the body mass of MPM-PV 17453, the humeral and femoral cross-sectional areas were calculated by multiplying midshaft maximum antero-posterior distance by maximum mediolateral distance from cross-sections obtained digitally in Avizo 3D (see Figure 4). This approach mimics calculating cross-sectional areas based on caliper measurements on physical specimens in the same axes, matching the body mass proxy data used by Pampush et al. (2021). The phylog-

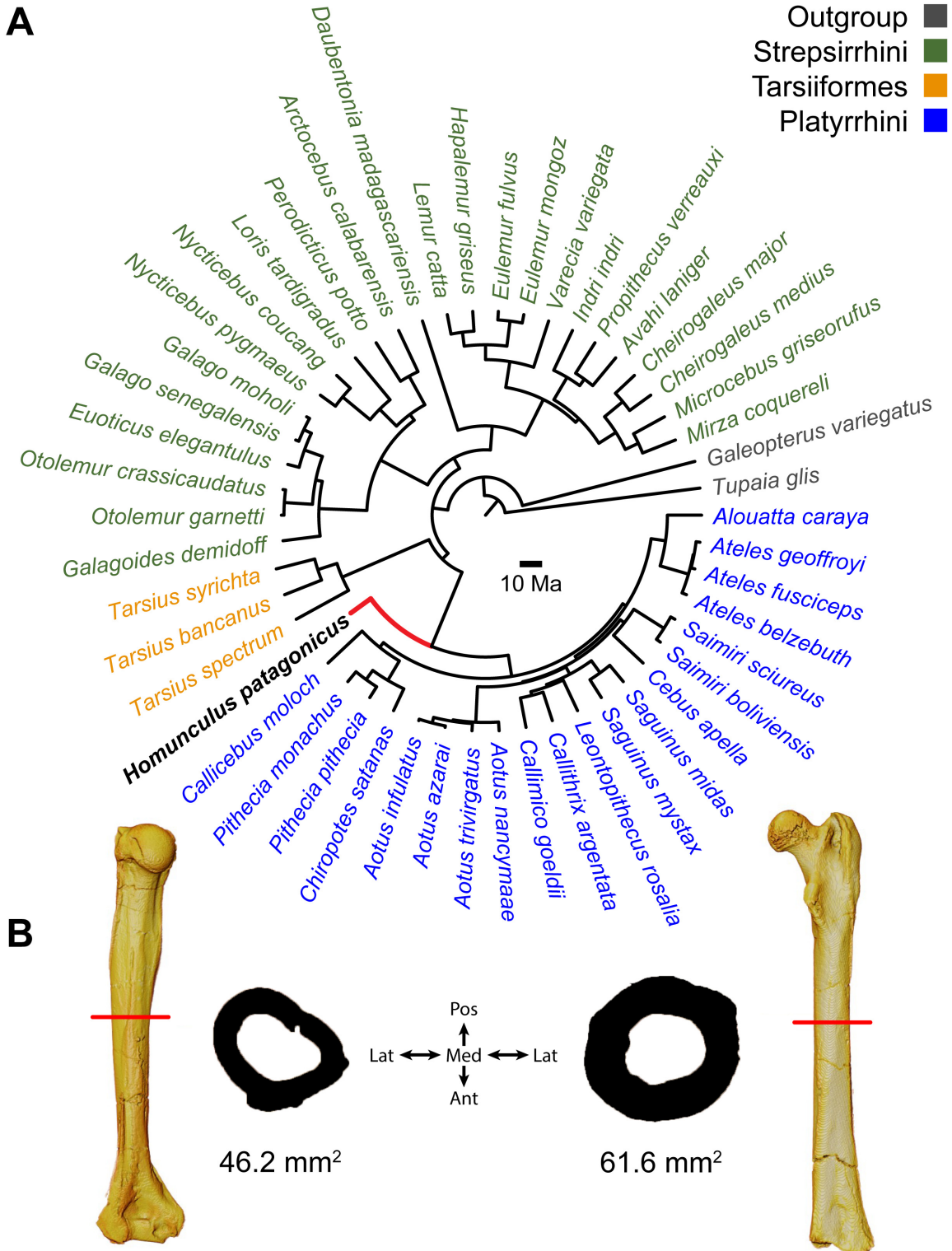


FIGURE 4. Body size estimation of MPM-PV 17453. **A:** Phylogeny utilized in the PIC analysis (Pampush et al., 2021). **B:** 3D reconstructions of the right humerus and right femur, both in posterior view. Red lines across the bone models indicate the locations where midshaft cross-sectional area was measured. Black silhouettes represent cortical bone at the cross section and area measurements represent the product of the maximum anteroposterior distance and the maximum mediolateral distance. Directional indications at center apply to the cross sections only, not to the 3D models.

eny used by those authors (derived from Yapuncich, 2017) was modified to include *Homunculus* as a stem platyrrhine, with a divergence from crown Platyrrhini at 28 Ma and a branch length of 11 Ma. Body mass estimations were derived for both the humeral and femoral cross-sectional areas using scripts for PIC provided by Pampush et al. (2021) and implemented in the R statistical computing environment (R Core Team) and averaged to obtain a body mass estimate for MPM-PV 17453 (Figure 4).

RESULTS

Anatomical Description

In the following section, elements that are well known from previously published specimens are given brief description only. Those that are new are described in greater detail.

Cranium. The cranium of MPM-PV 17453 is nearly complete; the only major component lacking is the lateral part of both the zygomatic arches (Figure 5). All teeth are present except the left I2; the left I1 is partly broken at the tip. There is some distortion in the face: there are cracks in the bone, and fragments have shifted slightly with respect to each other such that the rostrum is offset a little toward the left and the lateral margin of the right orbit is crushed inward slightly. The braincase appears to

be mostly undistorted. Natural cranial sutures are well preserved, including in the basicranium (although the metopic suture is well fused). The dentition is fully adult with no deciduous teeth present. There is substantial wear on all cheek teeth, less than in MPM-PV 3502, but more than in MPM-PV 3503 (both adult *Homunculus* crania from the same locality). The process of digital restoration yielded a symmetrical skull model (Figure 6).

Orbital and interorbital region. The right and left orbits with their postorbital septa are preserved intact in MPM-PV 17453, although there is substantial distortion of the right orbit. Orbital dimensions of MPM-PV 17453 and other *Homunculus* specimens are presented in Table 3. Relative to prosthion-inion length, the orbit dimensions are comparable to those of similarly sized extant platyrrhines suggesting a diurnal activity pattern.

Optic foramina and superior orbital fissures are preserved at the apex of the orbits in MPM-PV 3502. Digital removal of the matrix in MPM-PV 17453 reveals those foramina bilaterally. The right optic foramen is slightly crushed, but the left is intact and round. The size of the optic foramen is within the range expected for a crown anthropoid of the body size of *Homunculus* and is larger than those of strepsirrhines of similar size. The area of the optic foramen in MPM-PV 17453 is 3.7 mm² (calculated as the area of an ellipse with a major

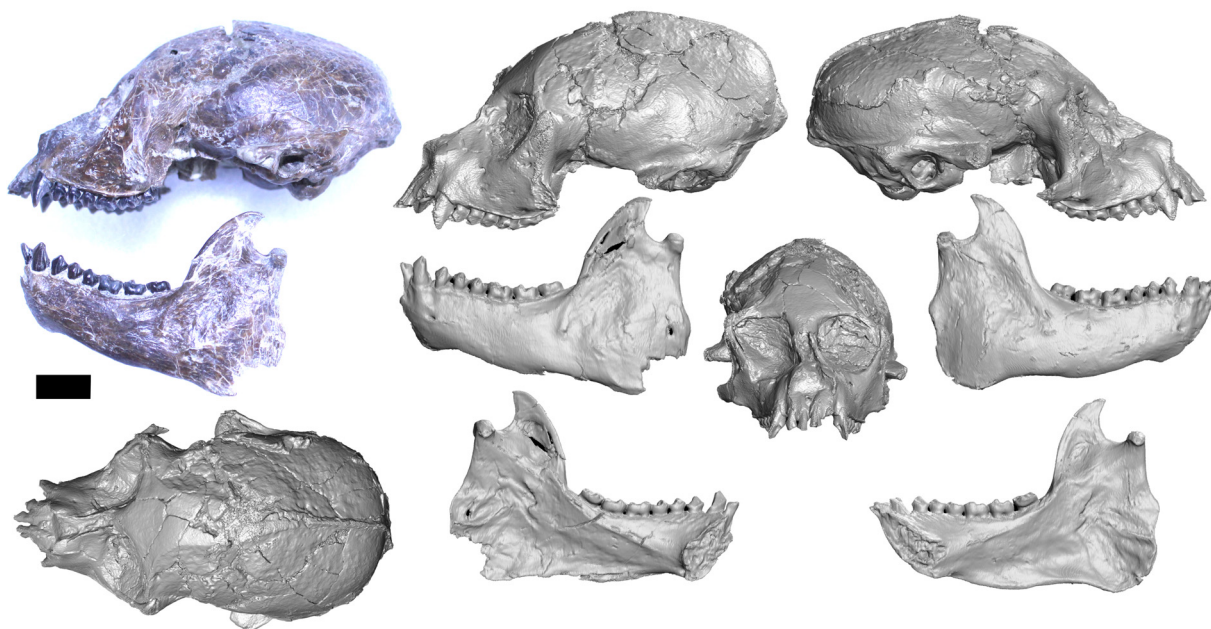


FIGURE 5. Skull of *Homunculus patagonicus* MPM-PV 17453 in various views. Scale bar equals 1 cm.

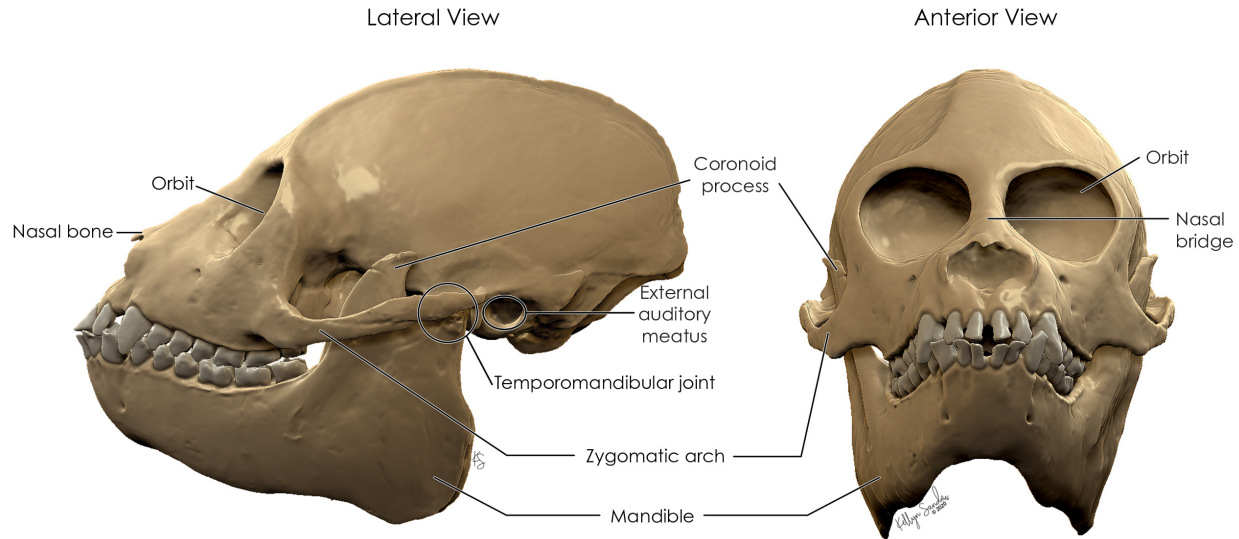


FIGURE 6. Restored skull of *Homunculus patagonicus* based primarily on MPM-PV 17453.

axis equal to 2.38 mm and a minor axis equal to 1.98 mm).

Several small and inconsistent foramina are located on the lateral side of the orbits but in no specimen of *Homunculus* (nor in *Tremacebus* or *Dolichocebus*) is there an enlarged zygomaticofacial foramen as is common to atelids and *Callicebus* (Horowitz and MacPhee, 1999).

The interorbital region and nasal cavities are exceptionally well preserved in MPM-PV 3502; its turbinates were described in detail by Lundeen and Kay (2022). The nasal is missing (bilaterally) on MPM-PV 17453, but it is present in MPM-PV 3502; it is narrow dorsally but wide ventrally.

In MPM-PV 17453, exposure of the maxilla on the ventral orbital margin separates the lacrimal from the zygomatic, as in all anthropoids. The right lacrimal fossa is exposed to the ventromedial margin of the orbit, but its sutures are not visible in adult specimens. In a juvenile specimen (MPM-PV 3503), the lacrimal fossa is composed of the maxilla rostrally and the lacrimal caudally. As the lacrimal fossa is completed anteriorly by the maxilla, the lacrimal bone remains within the orbit. An interorbital process of the maxilla is interposed between the lacrimal and nasal bones and reaches the frontal, thereby excluding the lacrimal from contacting the nasal. This pattern contrasts with that of CORD-PZ 1130, where the lacrimal extends onto the face to contact the nasal. CT cross sections show that the nasolacrimal duct is vertically oriented in both MPM-PV 3503 and CORD-PZ 1130,

as in other anthropoids. In CORD-PZ 1130, the lacrimal bone extends onto the face anterior to the orbital margin and contacts the frontal, thereby separating the maxilla from the frontal. Extension of the lacrimal onto the face anterior to the orbit is seen also to varying degrees in *Callicebus* and atelids.

Postorbital closure is complete in MPM-PV 17453 and MPM-PV 3502, as in CORD-PZ 1130. There is a lateral orbital foramen, identified by Hershkovitz (1977) as a remnant of the lateral orbital fissure, which, in *Tarsius*, extends laterally to the root of the zygomatic arch. This foramen is common in platyrrhines but rare in catarrhines (Hershkovitz, 1977). It is quite large in MPM-PV 3502, much larger than in *Aotus*. The apparently expanded infraorbital fissure in *Tremacebus* is largely due to postmortem breakage (Fleagle and Rosenberger, 1983; Kay et al., 2004).

As in all extant anthropoids, the orbits are convergent and frontated. Orbital convergence in two specimens was measured as in Ross (1993) with comparative data from Heesy (2003); it averages 66.5 degrees. This is within the range of extant platyrrhines of similar cranial size, and appreciably more convergent than similar-sized extant strepsirrhines. We calculate similar orbital convergence in *Dolichocebus* (71°) and *Tremacebus* (69°). The early catarrhine *Aegyptopithecus*, at 72° or greater (Ross, 1995; Simons, 2004), also had an extant anthropoid-like level of orbital convergence. Notably *Simonsius*, the only stem

TABLE 3. Cranial measurements^a of select *Homunculus* specimens.

	MPM-PV 17453	MPM-PV 3501	MPM-PV 3502	MPM-PV 3503	MPM-PV 3505	MPM-PV 5000 ^b
Cranial Length	75.58	68.82*	70.45*	72.87*	n/a	n/a
Cranial Breadth PB ^c	37.57	33.22	34.82	27.04*	31.81	30.16
Cranial Breadth PC ^d	31.03	24.39	25.28	28.28*	27.70	27.80
Facial Height ^e	10.85	11.71	10.82	11.15	8.06	9.48
Orbit Height ^f	14.03	14.85	14.66	16.60	12.75	14.01
Orbit Breadth ^g	14.38	14.30	13.45	9.78*	12.16	12.23
Interorbital Breadth ^h	6.11	5.06	4.20	5.52*	3.53	4.40
Orbital Convergence ⁱ	68	n/a	70	n/a	n/a	64
Foramen Magnum Length ^j	11.56	11.38	9.82	n/a	n/a	n/a
Foramen Magnum Breadth ^k	9.59	6.81*	9.14	n/a	n/a	n/a
Palate Length ^l	28.29	25.46	28.44	23.36*	24.99	25.80
Palate Breadth ^m	22.53	22.96	24.23	23.12	23.24	22.74
Geometric Mean ⁿ	18.43	16.88	17.00	18.85	14.76	15.60
Maxillary Depth ^o	7.45	7.93	10.93	n/a	n/a	11.54
Pre-orbital Rostral Length ^o	15.34	16.37	15.7	n/a	n/a	14.42

^aAll measurements are in millimeters except orbital convergence (degrees). Asterisk indicates the best estimate given distortion or breakage. This measurement is the maximum distance in the sagittal plane.

^bType of “*Killikaike blakei*”

^cMaximum right-to-left measurement at the postorbital bars.

^dOutside caliper measurement at deepest part of postorbital constriction.

^eVertical distance from inferior edge of orbital rim to inferior edge of alveolar process of maxilla at the distal (=posterior) edge of the P4.

^fMaximum inside dimension in vertical plane.

^gMaximum inside dimension in horizontal plane. Orbital measurements taken from the less distorted orbit of the two.

^hDistance between the most medial point on the left orbit and the most medial point on the right orbit.

ⁱIn degrees, as measured by Heesy, Ross, and colleagues (e.g., Heesy, 2003; Ross, et al., 2007).

^jMaximum inside dimension in the antero-posterior plane.

^kMaximum inside dimension in the mediolateral plane.

^lDistal edge of M3 to inferior nasal spine; direct distance.

^mBuccal edge of RM1 to buccal edge of LM1.

ⁿGeometric mean of all above available measurements. Missing measurements were not estimated. This underestimates the true size for the very incomplete specimens MPM-PV 3505 and MPM-PV 5000.

^oSee Ross (1994).

anthropoid to preserve this region, has remarkably less orbital convergence at 105° (Simons, 2001); adjusted for body size, the orbits of *Simonsius* are within the range of extant strepsirrhines, and outside that for any living or fossil anthropoid.

The interorbital region is quite narrow in MPM-PV 17453, as it is in all other *Homunculus* specimens, including MPM-PV 5000 (Table 3), as well as in *Dolichocebus* (Kay et al., 2008a). Coronal interorbital sections of *Homunculus* specimens

MPM-PV 17453 and MPM-PV 3502 show that the orbits are most closely approximated below the olfactory tract. As in most platyrrhines (except for *Saimiri*), an interorbital septum is composed of two laminae of bone. An interorbital opening in *Dolichocebus* is likely an artifact of preparation, not a resemblance to *Saimiri* (Kay, et al., 2008a), but see Rosenberger (1979a) for an alternate interpretation. In the latter, there is an interorbital fenestra

with its dorsal and ventral edges bounded by a single lamina of bone.

Nuchal region and exterior of neurocranium. As in all anthropoids, *Homunculus* has a pneumatized mastoid bone. The portion of the mastoid closest to the occipital protuberances is flattened as in *Dolichocebus* and *Tremacebus*, and in extant Cebidae. In contrast, pitheciines (Rosenberger, 1979b) and atelines have small paraoccipital processes. Theinion of *Homunculus* is dorsal relative to the foramen magnum, causing the nuchal plane to form an obtuse angle with the Frankfort Horizontal. This is typical of most living platyrrhines (Hershkovitz, 1977), as well as *Tremacebus* and *Dolichocebus*, but differs from the condition in *Cebus* and *Saimiri*, in which the nuchal plane forms a much more acute angle with the Frankfort Horizontal (Hershkovitz, 1977).

The sutures in the region of pterion are obliterated in MPM-PV 17453, which is a fully adult individual. MPM-PV 3502 exhibits the typical platyrrhine condition of parietal-zygomatic contact (Fulwood, et al., 2016). CORD-PZ 1130 apparently has the ‘catarrhine’ condition with the alisphenoid contacting the frontal, excluding a parietal-zygomatic contact. *Tremacebus* also has a parietal-zygomatic contact (Fulwood, et al., 2016). Neither *Tremacebus* nor *Homunculus* has a temporal emissary foramen.

On the side wall of the braincase of MPM-PV 17453, at the anteroposterior level of the posterior zygomatic root, the temporal lines meet and form a low sagittal crest, which reaches back to inion. The condition in MPM-PV 3502 is obscured by breakage. MPM-PV 3503 from PLC has well-developed temporal lines, which do not meet to form a sagittal crest. *Dolichocebus* lacks a sagittal crest, but the temporal lines are more closely approximated to the midline of the cranial vault than in *Saimiri*. *Tremacebus* has similar morphology to *Dolichocebus*. None of these taxa or specimens have the suprameatal foramen often found on the side wall of atelid crania.

Zygomatic region. The zygomatic arches are broken in MPM-PV 17453, with only the anterior and posterior roots preserved bilaterally. MPM-PV 3502 has a well-preserved right zygomatic arch, and MPM-PV 3503 has a well-preserved left zygomatic arch. The arch is robust dorsoventrally as in *Calli-cebus*. Its ventral border does not extend below the plane of the alveolar border as in extant platyrrhines except *Callicebus* where it is more ventrally displaced (Horovitz and MacPhee, 1999).

Temporomandibular region. The surface of the mandibular fossa, preserved on several crania, is broad and flat, with no indication of an articular eminence. Strong entoglenoid and post-glenoid processes are present. In contrast, *Dolichocebus* has a relatively small postglenoid process like *Saimiri* and callitrichines. *Tremacebus* likewise has a very small postglenoid process.

The right postglenoid foramen of *Homunculus* is situated posteromedial to the postglenoid process and is quite large, indicating that a large intracranial venous drainage channel (the petrosquamous sinus) emerged at this point (Saban, 1963; Conroy, 1980; Kay et al., 2008a). The foramen is smaller in similarly sized *Tremacebus*. *Dolichocebus* resembles *Homunculus* in having a relatively large foramen.

Pterygoid and palatal region. Distally, the postcanine tooth rows of *Homunculus* are parallel sided back to the M1, then diverge slightly, proportions that are like those of *Dolichocebus* and *Tremacebus*. Eocene/Oligocene anthropoids and many extant catarrhines have similarly nondivergent tooth rows, whereas the postcanine teeth of many crown platyrrhines diverge more markedly.

The palatine-maxillary suture reaches rostrally in the mid-sagittal plane to the level of M1. The distal margin of the hard palate is arched bilaterally such that the mesial apex of each arch is lateral to the midline. However, the posterior nasal spine is absent or indistinct. This condition, referred to as a ‘peaked’ choana (Rosenberger, 1985), is unlike the condition of most extant platyrrhines where the distal margin is straight, not arched. The palate of *Dolichocebus* is too damaged to establish this condition; that of *Tremacebus* is straight.

The pterygoid fossa, pterygoid plates, and the pyramidal processes are well preserved in MPM-PV 17453 and MPM-PV 3502. The pyramidal processes are situated laterally, just medial to the cheek teeth. There is a notch between the pyramidal process and the maxillary tuberosity. Both lateral and medial pterygoid plates are well developed. They are well separated from the auditory bulla, with the foramen ovale posterior and slightly lateral to the lateral plates. The posterior edge of the palatal processes of the palatine bone are slightly thickened to form a weak posterior palatine torus.

Facial region. The depth of the maxilla of *Homunculus* is comparable to that of most anthropoids. The distance from the left orbital margin to the anterior edge of the canine alveolus is 15.34 mm (preorbital rostrum length; [Ross, 1994]), and the

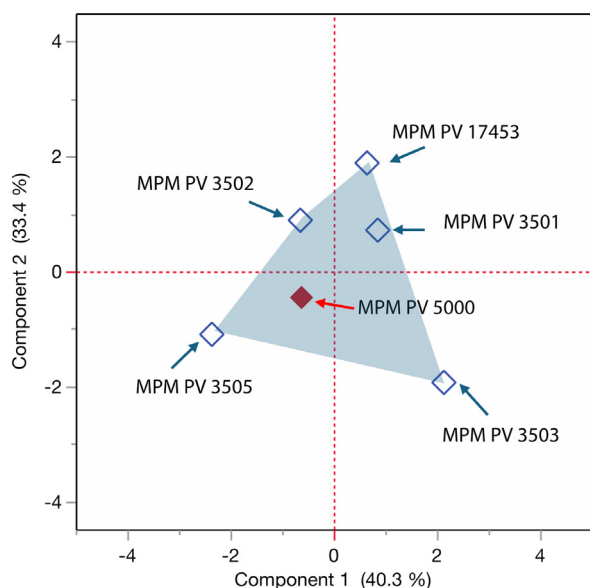


FIGURE 7. Principal components analysis of six dimensions of the face and orbits of *Homunculus*. Open blue diamonds represent five *Homunculus* crania. Closed red diamond is MPM-PV 5000, the specimen originally described as the type specimen of *Killikaike blakei*.

distance from the anterior edge of the canine alveolus to the nasomaxillary suture (maxillary depth [Ross, 1994]) is 17.45 mm. On the log-log plot in Ross (1994: fig. 17), these values plot in the middle of the anthropoid cluster. These measurements in *Dolichocebus* likewise plot with extant anthropoids of similar size. *Tremacebus* is too fragmentary to measure.

The area of the infraorbital foramen in MPM-PV 17453 is 0.91 mm² (calculated as the area of an ellipse with a major axis equal to 1.44 mm and a minor axis equal to 0.81 mm).

Homunculus had a 'long' snout as defined with Ross' measurements (pre-orbital rostrum length versus inion-canine length), much longer than that of extant platyrrhines. On the other hand, using Ross' plot (1994, fig 16), *Dolichocebus* and *Tremacebus* (accounting for missing parts) both appear to have a shorter rostrum, more akin to extant platyrrhines than extant strepsirrhines.

In view of the debate about the identity of MPM-PV 5000, whether it is a distinct taxon (*Killikaike blakei*, Tejedor et al., 2006) or rather belongs with other specimens of *Homunculus patagonicus*, we undertook a principal components analysis (PCA) of nine dimensions of the palate and orbits shared by MPM-PV 5000 and other specimens (Table 3: Facial Height, Orbit Height,

Orbit Breadth, Interorbital Breadth, Orbital Convergence, Palate Length, Palate Breadth, Pre-orbital Rostral Length, and Interorbital Breadth). The first two components account for 73.7% of the variance (Figure 7). Taken together, these data show that the shape of preserved parts of the face, palate, and orbits of MPM-PV 5000 fit within the known range of five other specimens of *Homunculus patagonicus*.

Ear region and braincase. The ear region is well preserved on both sides in MPM-PV 17453, MPM-PV 3502, and MPM-PV 3403. The petrosal roof of the middle ear is unexpanded and does not encroach on the basioccipital stem, nor does the basioccipital encroach on the petrosal externally. The posterior carotid foramen on the petrosal of *Homunculus* (marking the entrance into the bulla of a large internal carotid artery) is much the same as previously described in *Dolichocebus*. It is identifiable on the external surface of the petrosal, posterior to a line joining the midpoints of the ectotympanic elements, and medial to the midline of the auditory bulla, here established as a line joining the stylomastoid foramen and the antero-medial-most point on the petrosal, although it is located far forward of the stylomastoid foramen (Figure 8). The same position appears to be held for *Proteopithecus*, *Catopithecus*, and parapithecids. In the stem catarrhine *Aegyptopithecus*, the posterior carotid foramen is also positioned posteriorly but more nearly in the middle of this line (Kay et al., 2008b). Inside the bulla, a ridge on the ventrolateral surface of the promontorium marks the presence of a bony tube for the internal carotid (promontory) artery.

The ectotympanic bone is extrabullar, forming a bony ring at the entrance to the tympanic cavity, and is fused to the exterior of the petrosal. This condition resembles early Oligocene stem anthropoids from Africa, as well as all known extant and extinct Platyrrhini (Kay et al., 2008b). The ring is ossified outward to form a tube in Miocene-Recent catarrhines (only partially so in *Aegyptopithecus* and *Pliopithecus*) and *Tarsius* (Szalay and Delson, 1979; Fleagle and Kay, 1987; Simons et al., 2007).

The right middle ear cavity and its anterior accessory chamber are exposed in a virtual cut-away in Figure 9. As in most platyrrhines, except atelids and *Cacajao* (Horovitz, 1997), *Homunculus* (like *Dolichocebus* and *Tremacebus*) possesses two prominences on the lateral surface of the promontorium. These prominences are the external manifestations of the cochlea on the promontory. The dual nature of these prominences may be

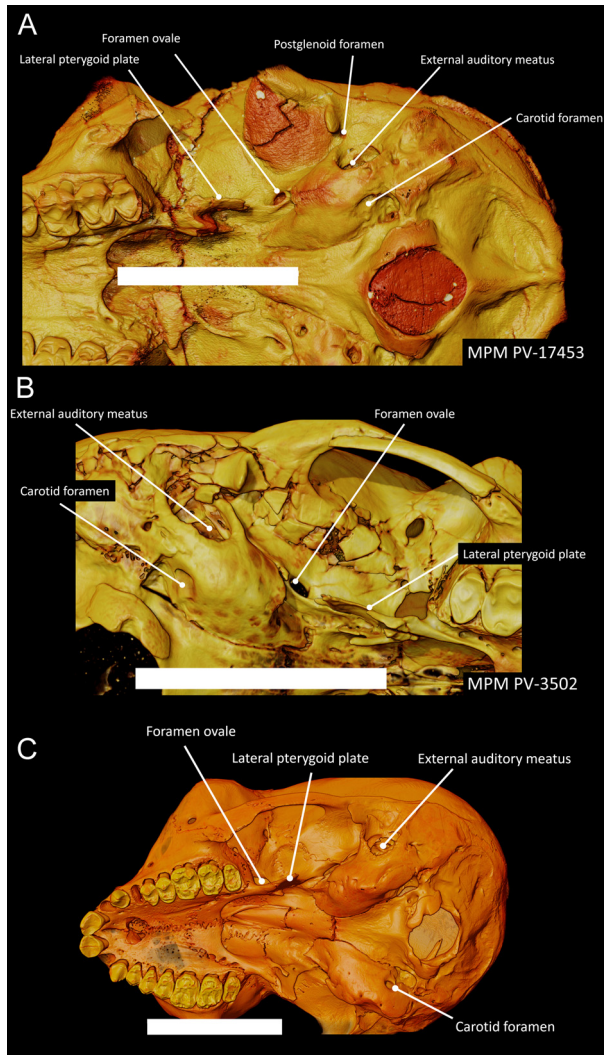


FIGURE 8. Basicranium of *Homunculus* specimens with an extant platyrrhine comparison. The white scale bar is 2cm long for each. **A:** MPM-PV 17453, **B:** MPM-PV 3502, **C:** extant *Plecturocebus*.

a derived feature of platyrrhines that was subsequently lost in atelids. This is supported by the observation that *Tarsius*, *Aegyptopithecus*, and *Simonsius* each have a single prominence (Kay et al., 2008). However, there are paired prominences on the cochlear housing in the middle ear in *Apidium* (see Cartmill, et al., 1981: fig. 1). Moreover, there is intraspecific variation in this feature in extant *Saimiri*, *Cebus*, and *Aotus*.

Middle ear morphology is typical of haplorhines in that a transverse septum separates the tympanic cavity proper from a well-developed anterior accessory chamber (AAC) (Cartmill and Kay, 1978; MacPhee and Cartmill, 1986). The latter develops as a diverticulum from the auditory tube (Ross, 1994). The AAC extends more medially and

has trabeculae within it, as in other anthropoids (Ross, 1994). Medial extension of the AAC is a derived feature of crown and stem anthropoids: It is a feature of the stem catarrhine *Aegyptopithecus*, and stem anthropoids *Apidium* and *Simonsius*, as well as *Proteopithecus* and *Catopithecus* (Kay et al., 2008b).

Serial CT sections of the petrosals of several crania, particularly MPM-PV 3503, show Cartmill's canal, a narrow venous channel connecting the subarcuate fossa with the sigmoid sinus (Cartmill et al., 1981; Kay et al., 2008a). This is present in all platyrrhines, including *Dolichocebus* and *Tremacebus*. It is absent in *Tarsius*. The canal is present and well developed in the stem anthropoids *Proteopithecus* and *Catopithecus* (Kay et al., 2008b). It is absent in the Oligocene parapithecids *Apidium* (Cartmill et al., 1981) and *Simonsius* (Kay et al., 2008b). It is partially obliterated in the stem catarrhine *Aegyptopithecus*, but is absent in crown catarrhines

Interior of braincase and brain size. MPM-PV 3502 and MPM-PV 17453 have an ossified tentorium cerebelli (fragmented in MPM-PV 17453); this is visible on coronal CT slices through the braincase, bilaterally above the subarcuate fossa. The tentorium is also visible in *Dolichocebus* (Kay et al., 2008a). Horovitz and MacPhee (MacPhee et al., 1995; Horovitz, 1999; Horovitz and MacPhee, 1999) stated that the tentorium is absent in *Tarsius* (and sometimes absent in *Saimiri*) but present in all other platyrrhines. An ossified tentorium is also absent in *Aegyptopithecus* and in *Apidium* (Kay et al., 2008b). In contrast, Hershkovitz (1977) noted that it is most extensive in the extant platyrrhines *Ateles*, *Lagothrix*, and *Brachyteles*; peripheral in *Callicebus*, *Aotus*, and pitheciines; variable in *Alouatta*; minimal in *Saimiri*, *Cebus*, and *Callimico*; and absent or rudimentary in other callitrichines. Our observations on additional extant platyrrhine crania support Hershkovitz's observations for the most part. However, CT images show the tentorium to be quite well developed in *Callimico*.

On all adult specimens of *Homunculus* examined, the metopic suture is fused. A slight depression is found at glabella above weak brow ridges. The glabella is also slightly depressed in *Tremacebus*; the shape is indeterminate in *Dolichocebus* where the bone is absent.

Two specimens were sufficiently complete to estimate an endocranial volume: MPM-PV 17453 has an estimated endocranial volume of 21,831 mm³ with an olfactory bulb volume of 54.6 mm³, and MPM-PV 3502 has an estimated endocranial

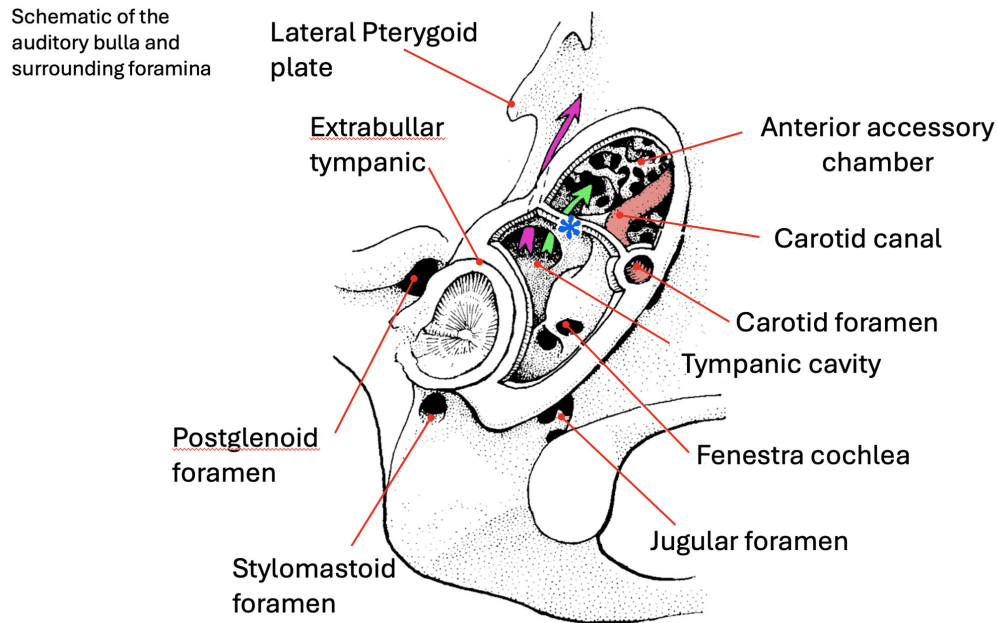


FIGURE 9. Schematic of the right ear region in ventral view. Anterior is toward the top of the image and lateral is toward the left margin. The purple arrow is the connection between the middle ear cavity and the pharynx via the auditory/pharyngotympanic tube. The green arrow is the connection between the middle ear cavity and the anterior accessory chamber. The asterisk labels the bony partition separating the middle ear cavity from the anterior accessory chamber. Redrawn after Cartmill et al. 1981: fig.10B.

volume of 20,036 mm³ with an olfactory bulb volume of 37.9 mm³. Considering a range of body mass estimates (see below) these volumes are very small for an extant platyrrhine but fall within the range for extant strepsirrhines (Figure 10). Compared with overall brain volume, the olfactory bulbs are large for an extant anthropoid but do not reach the size attained by *Aotus* in this respect.

However, the bulbs are proportionately smaller than in extant strepsirrhines.

The size of the frontal lobe of *Homunculus* has been a subject of debate. Based on the partial cranium CORD-PV 1130, Tauber (1991) stated that the frontal lobe is 'highly developed' but made no direct comparisons to extant taxa. Tejedor et al. (2006), in their account of the facial skeleton of

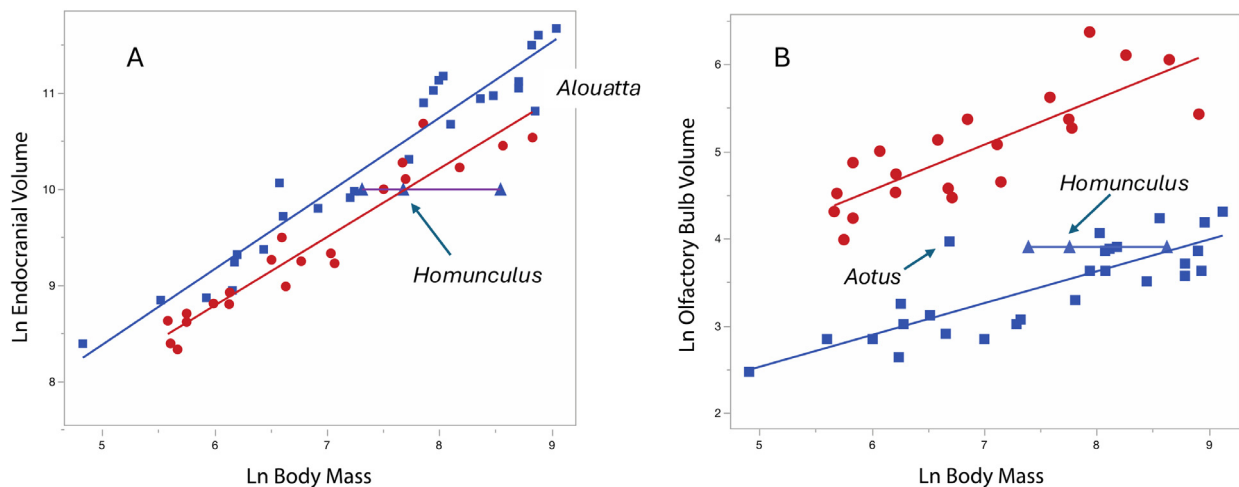


FIGURE 10. Bivariate logistic plots of body mass versus brain size (A) and olfactory bulb size (B) for extant genera of Platyrrhini (blue squares) and Strepsirrhini (red dots) with *Homunculus* shown as a range depending on the estimated body size.

MPM-PV 5000, estimated the volume of the frontal lobe based on the volume of the anterior cranial fossa rostral to the optic foramina, and concluded that the forebrain was large like in the extant platyrrhine *Saimiri*, and larger than that of the extant platyrrhine *Callicebus*. They further claimed that because the frontal lobe was large, the brain must also have been large, drawing a special similarity between MPM-PV 5000 and extant cebine platyrrhines. By comparison, they stated that the frontal bone and anterior cranial fossa of CORD-PV 1130 resembles the extant pitheciine *Callicebus* and differs from the 'vaulted frontal' of MPM-PV 5000 and living cebines. Kay and colleagues (2012) briefly described several other *Homunculus* crania, especially MPM-PV 3502 from the same locality as MPM-PV 5000. They suggested that the frontal lobe must have been small compared with most platyrrhines, based on its very low frontal profile in the mid-sagittal plane, compared with similar-sized extant platyrrhines (see Kay et al., 2012, fig. 16.8). They noted that the facial skeleton of *Homunculus* is upwardly rotated on the neurocranium in their specimens, a condition described as airorhynch (Tattersall, 1972). They concluded that, after accounting for airorhynch, the frontal of MPM-PV 5000 is not 'domed', and the forebrain is not expanded.

Mandible. The mandible of MPM-PV 17453 (Figure 6) is the most nearly complete of any specimen of the species, on both sides, lacking only the left i1 and a small piece of the mandibular angle on each side. It is broken just to the left of the fully fused symphysis. The medial pole of the mandibular condyle is tubular as seen from above, but its upper edge is markedly convex, and it projects more medially from the condylar neck than it projects laterally (i.e., its inferred center of mass is medial to the neck of the condyle). In most respects, it greatly resembles the two other most complete mandibles of *Homunculus* (MPM-PV 3504 and MPM-PV 3708). The condyle of the new specimen is slightly longer (antero-posteriorly) than that of MPM-PV 3708, giving the latter a more tubular appearance. As with other specimens of *Homunculus*, the mandible of the new specimen has prominent fossae for the anterior digastric muscle, the medial pterygoid muscle, and the deep temporalis muscle. The medial pterygoid fossa bears two (or more) prominent ridges for the insertion of intramuscular fasciae of the medial pterygoid muscle. There is a distinct fossa for the insertion of the lateral pterygoid muscle on the medial side of the condylar neck. The long axis of the mandibular

symphysis is at a roughly 45° angle to the occlusal plane. The mandible of MPM-PV 17453 deepens slightly posteriorly (comparing p2 depth with m3 depth), as in MPM-PV 3504 and MACN-A 5757. This degree of deepening is like that in *Aotus*, but not to the degree seen in pitheciids where substantial deepening occurs (see Kay, 1994: Table 3).

Dentition. All teeth are present except the left I2 and left i1; the left I1 is partly broken at the tip (Figure 11). The dentition is fully adult. There is wear on all cheek teeth, less so than in MPM-PV 3502 but more than in MPM-PV 3503 (both adult *Homunculus* crania from the same locality). Other *Homunculus* specimens preserve a complete upper or lower incisor and canine series (MPM-PV 3502 and 3504), but none preserves both upper and lower teeth. Dental dimensions are presented in Tables 4 and 5.

Upper teeth. Many details of the crown anatomy of the upper teeth are obscured by *in vivo* wear but, where preserved, the details resemble MPM-PV 3502, MPM-PV 3505 (a juvenile specimen), and MPM-PV 5000.

As with MPM-PV 3502, the upper central incisor crown of MPM-PV 17453 is spatulate and the cross-section of its root is labio-lingually broad, suggesting that it was optimized to resist powerful labio-lingual bending stresses engendered during ingestion. The upper lateral incisor is more pointed but functioned with the upper central in edge-to-edge incision. The incisors are separated from the canine by a substantial gap.

The upper canine crown has a strong lingual ridge running from the apex to the base of the crown. This ridge separates a deep mesial groove from a shallow groove distally.

The upper premolars have oval occlusal outlines, slightly wider buccally than lingually. The paracone is tall in P2 and a small protocone is present lingually. The postparacrista is short and there is no hypocone. The P3 and P4 are similar in each having a cristiform paracone and well-developed protocone with a hypocone on a distal marginal cingulum.

The first and second upper molars are heavily worn but where preserved they resemble the structure of MPM-PV 3505. Each is four-cusped. On M1 the metacone is nearly as large as the paracone; on M2 the metacone is slightly smaller than the paracone. On both teeth, the metacone and paracone are widely separated, leaving the postparacrista and premetacrista much longer than the preparacrista and postmetacrista. All four buccal crests are aligned mesiodistally. Details of the sty-



FIGURE 11. Left upper and right lower dentition of *Homunculus patagonicus* MPM-PV 17453 from high resolution CT stacks at 70 microns. Scale bar equals 1 cm.

lar cusps are obliterated, as are the details of the crown where the paraconules and metaconules would have been present. Arising from the protocone is a strong preprotocrista that joins the preparaconule crista. The hypocone is large, distal, and slightly lingual to the protocone on M1-2. There is a prominent prehypocrista that directly connects with the wall of the postprotocrista, closing off the talon lingually. The posthypocrista is strong and apparently confluent with a distal cingulum.

There is no buccal cingulum on M1-2. A well-developed lingual cingulum runs mesiolingually from the apex of the hypocone around the base of the protocone, delineating a wide cingular shelf before joining the preprotocrista. The lingual cingulum is unadorned by a pericone or another cusp.

M3 has a rectangular occlusal outline, wider (buccolingually) than it is long. It lacks a hypocone, but there is a deep groove between the protocone and the strong (deeply incised and wide) lingual cingulum. The metacone is small and the paracone is very tall by comparison.

Molar size decreases from M1 to M3, with M3 being less than half the area of M1. M1-2 has two buccal roots and one lingual root. M3 is two-rooted.

Lower teeth. The best-preserved incisors are those of MPM-PV 17453 and MPM-PV 3504; MPM-PV 3508 has an i2. The lower incisors of MPM-PV 17534 resemble those of MPM-PV 3504 (the best preserved lower anterior dentition), albeit much more heavily worn. These teeth are spatulate, slightly procumbent, and moderately elongate from the cemento-enamel junction to the cusp tip, reminiscent of the condition seen in *Callicebus* or *Saguinus*. The lower first incisor is smaller than the i2, as in all anthropoids. Both incisors support a ribbon-like occlusal facet for an edge-to-edge bite with the upper central incisor. Neither tooth has a lingual cingulum. I2 has a discrete heel distally.

The canines of *Homunculus* are small relative to the molars, do not project far above the premolar tooth row, and are separated from the incisors by a short diastema. In these respects, the greatest structural similarity is with living *Callicebus* or *Aotus*. The small canines would have been useful tools for food incision—separation of a bite—but not in the fashion seen in several platyrrhines in which that tooth is enlarged (pitheciines) or incorporated in the gouging mechanism (callitrichines).

Assessment of the premolars relies primarily on MPM-PV 3508 because these teeth are more worn in MPM-PV 17453 and MACN-A 5757. The following description, therefore, pertains to all known *Homunculus patagonicus* specimens, except as noted. The p2-4 are single rooted, a common feature of all extant and extinct platyrrhines whereas p3-4 are two-rooted in African anthropoids, including all those from the late Eocene and early Oligocene (parapithecoids, proreopithecids, and oligopithecids sensu Seiffert, 2012). The premolar crowns increase in size distally; they are (mesiodistally) short and (buccolingually) wide, and p4 is small relative to m1. The crowns are slightly inflated and lack buccal or lingual cingula.

The p2 does not project above the occlusal row; MPM-PV 5757 and MPM-PV 17453 lack a discrete p2 metaconid; that tooth is broken in MPM-PV 3708. The p3 lacks a distinct paraconid (seen in MPM-PV 3708 only; too worn to be assessed in MPM-PV 17453 and MPM-PV 5757). A p3 metaconid is present on all specimens but is lower than the protoconid and positioned distolingually such that the lateral protocristid is distolingually oriented. The talonid is low and distinct. The entoconid is the largest talonid cusp and projects above the hypoconid (visible in MPM-PV 3708).

The p3 is slightly smaller than p4; the p3-4 protoconids are equal in height. The p4 lacks a dis-

TABLE 4. Lower tooth dimensions^a for *Homunculus patagonicus*, including MPM-PV 17453.

Specimen number	i2 m-d								
	i1 m-d	i1 m-d root	i1 b-l	i2 m-d	i2 m-d root	i2 b-l	/c m-d	/c b-l	/c height
MPM-PV 17453	1.62	n/a	2.06	2.62	n/a	2.43	3.48	3.28	4.12
MPM-PV 3504	1.88	1.49	2.04	2.68	1.53	2.45	3.91	2.84	6.11
MACN-SC 3114	1.62		2.32						
MPM-PV 3708							3.54	3.6	
MACN-A 634 ^b							3	3.1	
	p2 m-d	p3 b-l	p3 m-d	p4 b-l	p4 m-d	p4 b-l			
MPM-PV 17453	4.62	2.76	3.34	3.4	3.6	3.7			
MPM-PV 3504	3.68	3.05							
MPM-PV 3708	3.02	3.36	3.47	3.15	3.56	3.54			
MACN-A 634 ^b	3.5	3.2	3.2	2.7	3.2	3.1			
MACN-A 5757 ^c	3.34	2.67	3.42	2.85	3.08	3.38			
MACN-SC 2916			3.2	4.78					
MACN-SC 3026					3.83	3.34			
MACN-SC 3116	3.51	2.98							
	m1 trigonid b- m1 talonid			m2 tal			m3 tri		
	m1 m-d	l	b-l	m2 m-d	m2 tri b-l	b-l	m3 m-d	b-l	m3 tal b-l
MPM-PV 17453	4.37	4.13	4.34	4.45	3.94	3.82	4.24	3.82	3.14
MPM-PV 3504				5.12	4.67	4.69	4.28	3.78	2.94
MPM-PV 3708	4.81	4.1	4.19	4.84	3.96	3.75	4.73	3.87	3.3
MPM-PV 4376	4.18	3.58	3.51	4.24	3.39	3.31			
MLP-PV 11-121	4.23	3.52	3.67						
MLP-PV 55-XII-13-156	4.24	3.39	3.75						
MACN-SC 3200							3.48		
MACN-SC 334	4.55	3.55	3.58						
MACN-SC 336	4.28	3.51	3.76	4.35	3.5	3.45			
MACN-SC 338	4.46	3.62	3.41						
MACN-SC 339	4.3	3.69	4.03	4.29	3.72	3.61			
MACN-SC 341	4.41	3.58	3.74						
MACN-SC 3074	4.32								
MACN-SC 3090				4.27	3.4	3.36			
MACN-SC 2918				4.31	3.56	3.4			
MACN-SC 1149				4.28	3.46	3.34			
MPM-PV 19428*	4.12	3.5	3.51	4.31	3.5	3.51			
MPM-PV 17452							4.73	3.55	2.86
MACN-A 10403	4.42	3.59	4	4.32	3.69	3.65			
MACN-A 5757 ^c	4.38	3.5	3.8	4.27	3.49	3.6	4.23	3.45	2.92
MACN-A 5966				4.24	3.63	3.45			
MACN-A 5969 ^d	4.43	3.71	3.87	4.4	3.59	3.64			
MACN-A 634 ^b	4	2.8	3.2	4.5	3	3.5			
MPM-PV 17487				4.88	3.7	3.51			
MPM-PV 19426*	4.17	3.35	3.44						

^aAll measurements are in millimeters. ^bFrom Rusconi (1935) ^cRight side. ^dComposite of a and b. Asterisk indicates specimens that belong to *H. vizcainoi*, including the Type specimen (MPM-PV 19426); all others are *H. patagonicus*.

TABLE 5. Upper tooth dimensions^a for *Homunculus patagonicus*, including MPM-PV 17453.

Specimen number	I1 m-d			I2 m-d			C/ m-d	C/ b-l	C/ height
	I1 m-d	root	I1 b-l	I2 m-d	root	I2 b-l			
MPM PV 17453 ^b									
MPM-PV 3502	3.45	2.58	2.16	3.22	2.24	2.09	3.48	2.97	3.99
MACN-A 5968							3.61	3.22	
MACN-SC 275							3.87	3.36	4.76
MACN-SC 335 (or 355)							3.88	3.18	5.23
MACN-SC 3089	2.95	1.82	1.95						
MPM PV 5000							3.34	2.685	4.98
	P2 m-d	P3 b-l	P3 m-d	P4 b-l	P4 m-d	P4 b-l			
MPM-PV 17453 ^b	2.62	3.89	3	4.67	3.32				5.13
MPM-PV 3501	3.24	3.91	2.93	4.51	3.38				5.23
MPM-PV 3502	2.47	3.62	2.98	4.51	3.11				4.9
MPM-PV 3503	3.28	3.67	3.13	4.3	3.14				4.99
CORD-PZ 1130	2.7	3.5	2.6	4.4	2.9				5.1
MACN-SC 2916			3.17	4.76					
MACN-SC 3116	3.56	3.25							
MPM-PV 5000	2.795	3.46	2.98	3.87					
	M1 m-d	M1 b-l	M2 m-d	M2 b-l	M3 m-d	M3 b-l			
MPM-PV 17453 ^b	4.58	5.95	4.2	5.88	3.02				4.87
MPM-PV 3501	4.27	6.2	4.15	6.06	3.03				5.04
MPM-PV 3502	4.19	6.28	4.15	5.91	2.96				4.77
MPM-PV 3503	4.59	6.15	3.91	6.07	2.94				4.77
CORD-PZ 1130	3.77		3.75		2.62				
MACN-SC 274					3.07				4.8
MACN-SC 334			3.98	5.34					
MACN-SC 337			3.83	5.17					
MACN-SC 342			3.78	5.42					
MACN-SC 3012			4.01						
MPM-PV 5000	4.29		3.80	4.84	2.87				4.38
MPM-PV 1607 ^c	4.1	5.7	3.7	4.9	2.9				4.5

^aAll measurements are in millimeters.

^bMean of left and right values, except for I2 for which the left-side tooth is lost.

^cMeasurements from Tejedor et al. (2008).

crete paraconid; in its place is a slight raised ridge on the mesial margin of the trigonid (visible in MPM-PV 3708 only). There is a large metaconid, only slightly lower than the protoconid; the former is widely spaced from, and positioned distolingually to, the protoconid with a distolingually-oriented protocristid. The protocristid is not transversely oriented as is common among platyrrhines. There is no premetacristid, leaving a widely open trigonid. There is no postprotocristid, and the postmetacristid is only moderately developed. The entoconid is

a small discrete cusp, albeit the largest of the talonid cusps. The entire talonid basin is at the level of, or slightly lower than, the m1 trigonid. The hypoconid, which is distolingually positioned relative to the protoconid, supports a weak cristid obliqua, but the hypocristid is absent.

The m1-3 have the following features in common. There are two roots and there is moderate basal inflation; there is no buccal cingulum. Molar cusps are marginally positioned such that the trigonid and talonid basins are nearly as broad as the

entire crowns. In all lower molars, the paraconid is absent or crestiform (though not in *H. vizcainoi*, which has a large, centrally placed m1 paraconid: Kay and Perry, 2019). The hypocristid is moderate in size. The entoconid is large and is aligned transversely with the hypoconid.

The m1 and m2 have the following features in common. They are square shaped. The trigonids and talonids are of similar widths and heights. The trigonid is open lingually and the premetacristid is absent. The metaconid is transversely or slightly distolingually oriented. The cristid obliqua is strong; it reaches the posterior trigonid wall distolingual to the protoconid and runs partway up the posterior trigonid wall. The hypoconulid is weak or absent; when present, it is located on the distal margin of the crown slightly lingual to the crown's midline.

In the m3, the trigonid is wider than the talonid. The cristid obliqua is oriented more laterally than in the other two molars, and it reaches the posterior trigonid wall distal to the protoconid. There is a small distal lobe supporting a centrally placed hypoconulid.

Humerus. A complete right humerus and a partial left humerus are present in MPM-PV 17453 (Figure 12, Table 6). The left humerus represents approximately the distal 75% of the humerus. The right humerus is the first complete humerus known for *Homunculus*, and the first to preserve the proximal end (humeral head, tubercles). Previously the most complete humerus for the species was another mostly complete right humerus, MPM-PV 3500, from the same locality. The new right humerus demonstrates that the slightly smaller humerus MPM-PV 3500 is about 85% complete and it confirms previous reconstructed length estimates of 89-94 mm for MPM-PV 3500 (Fleagle et al., 2022). The humeri belonging to the new specimen reinforces the body size and locomotor inferences based on MPM-PV 3500 as they conform in every observable respect to the anatomy of the former (see further description below).

The MPM-PV 17453 humeri are very robust compared to living and some fossil platyrrhines (e.g., *Cebupithecia*; Meldrum et al., 1990). The surface anatomy conforms closely in overlapping



FIGURE 12. Humeri and scapulae of *Homunculus patagonicus* MPM-PV 17453. Original photos are shown along with the CT surface reconstructions for the more complete humerus and for the scapulae. Scale bar equals 1 cm.

TABLE 6. Measurements^a of humeri of *Homunculus*.

	MPM-PV 17453 (L)	MPM-PV 17453 (R)	MPM-PV 3500
Maximum length	82.07*	98.61	92
Maximum midshaft diameter	9.08	8.71	8.37
M-d midshaft diameter	6.32	6.42	6.64
A-p midshaft diameter	7.15	7.35	6.20
Bi-epicondylar width	21.49	20.43	20.24
Medial epicondyle angle	22	21	22
Capitulum depth	7.35	6.64	7.01
Humeral head superoinferior	n/a	13.01	n/a
Humeral distal mediolateral	15.28	14.54	14.30

^aHumeral head measurements are used to estimate body mass (see Perry et al., 2018). Except for the humeral midshaft diameters, all others are from Fleagle et al. (2022), based on measurements described in Fleagle and Simons (1982; 1995). All measurements in millimeters except medial epicondyle angle which is in degrees. Asterisk denotes a minimum measurement in the case of breakage.

parts to the previously studied humeral specimens (e.g., Fleagle et al., 2022). The deltopectoral and deltotriceps flanges are long and prominent, delimiting a laterally oriented deltoid plane. The attachment for teres major is large. At the distal end, the entepicondylar foramen is large and the medial epicondyle projects dorsally only to a moderate degree, commensurate with generalized arboreal quadrupeds (Fleagle and Kay, 1983; Fleagle et al., 2022). The brachialis flange is broad, and the supinator crest extends far proximally; the trochlear capitulum has a small but prominent tail; the trochlea is gently conical with a relatively sharp medial crest and a relatively blunt lateral edge; the trochlea lacks a clinging facet (Szalay and Dagosto, 1980). The lack of such a facet is consistent with *Homunculus* not having been a habitual vertical climber and leaper with highly flexed elbow postures (e.g., see Fleagle and Lieberman, 2015).

Especially noteworthy are the anatomical features of the proximal humerus as these have not been observed before. The articular head resembles that of *Pithecia* in overall shape and size. However, it is somewhat narrower mediolaterally and longer dorsoventrally. This suggests somewhat more excursion in flexion/extension than in mediolateral rotation. The long axis of the articular surface (greatest path length) is angled somewhat, such that the inferior end of the articular surface sits medial to the superior end of the articular surface. This suggests that as the humerus was flexed (swung anteriorly) relative to the scapula, the distal humerus was pronated. This could be adaptive in the context of climbing a vertical support hand-over-hand. Other features of the humerus of *Homunculus*, especially the configuration of the

deltoid plane, suggest the importance of using vertical supports (Cooke et al., 2016; Fleagle et al., 2022).

The greater tubercle is large and high, nearly reaching the summit of the articular head. A prominent lip demarcates the border between the insertion of the supraspinatus and infraspinatus muscles. There is a prominent dimple for the insertion of infraspinatus, below which is a small knob for the insertion of teres minor. The lesser tubercle is also prominent, nearly as high as the greater tubercle, with dimpling that likely represents a strong insertion for subscapularis. The overall look of the proximal end is like that of pitheciines (see Fleagle and Meldrum, 1988). This suggests both significant mobility and stability in the glenohumeral joint, commensurate with a locomotor style of generalized arboreal quadrupedalism (Fleagle and Simons, 1982; Fleagle and Simons, 1982; Fleagle and Simons, 1995), with perhaps an emphasis on climbing on vertical supports. Overall robusticity is high in *Homunculus*. This might suggest that body mass was high relative to support size (requiring more strength generally). It might also suggest that ideal supports were widely dispersed (requiring more climbing down to the ground and back up into the next tree) or that environmental conditions (high winds and precipitation, requiring stronger clinging to remain attached) or social conditions (inter-individual competition) contributed to the physical challenges encountered by *Homunculus*. Additional study is needed to infer relative sizes of limb muscles based on size and configuration of muscle scars and attachment features.

Scapula. The scapula of *Homunculus* was previously unknown. The new specimen preserves a fragmentary scapula from both the right and left sides. Both scapulae preserve a complete glenoid fossa but are broken medially. In both cases, the acromion is broken at its base; on the left the coracoid process is also broken at its base, but on the right the coracoid process is intact. The left scapula preserves more of the medial aspect. The only other Early Miocene scapula is a less-intact specimen from the Cerro los Toldos locality 4, Pinturas Formation (Anapol and Fleagle, 1988). That specimen (MACN-SC 101) is associated with a facial fragment (MACN-SC 100) currently attributed to *Carlocebus carmenensis* but might belong to a new genus and species (Novo et al., 2021). MACN-SC 101 also preserves a complete glenoid fossa but is broken away medially and at the bases of the coronoid and acromion processes.

The glenoid fossa of the scapula in MPM-PV 17453 is pear shaped. It is deeply concave as viewed from anterior, with a sharp angle separating a superior plane and an inferior plane. This is very similar to the glenoid fossa of MACN-SC 101. The scapular spine intersects the plane of the glenoid about one-third to one-quarter of the way up the glenoid. The coracoid process is robust, long, and tightly hooked, turning sharply laterally as it descends distally; its robusticity signals powerful shoulder flexors. A broad surface on the ventral aspect of the scapular blade marks the origin of

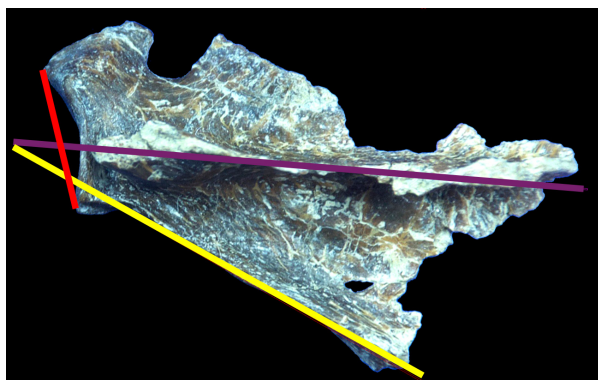


FIGURE 13. Left scapula of *Homunculus patagonicus* MPM-PV 17453 showing planes in posterior view for angular measurements. The yellow line is the axillary border, the purple line is the spine of the scapula, and the red line is the plane of the glenoid fossa. The axillo-glenoid angle is the obtuse angle at the intersection of the yellow and red lines, the axillo-spinal angle is the acute angle at the intersection of the yellow and purple lines, and the spino-glenoid angle is the obtuse angle at the intersection of the purple and red lines.

teres major; this is a very well-defined and very ventral surface, like that of pitheciines (Fleagle and Meldrum, 1988) that is also present in extant *Saimiri* and the African early Oligocene parapithecoid *Apidium* (Anapol, 1983). There is no visible ridge marking the border between the origins of infraspinatus and teres minor, though it is possible that such a ridge was present more medially.

Five measurements were taken on the scapulae of MPM-PV 17453, following Anapol (1983) and Anapol and Fleagle (1988). These are glenoid fossa height, glenoid fossa width, axillo-glenoid (AG) angle, axillo-spinal (AS) angle, and spino-glenoid (SG) angle (Figure 13, Table 7). The height of the glenoid fossa is very similar to that of MACN-SC 101 (right: 11.93 mm and left: 12.03 mm, compared to 13.20 mm in MACN-SC 101; Anapol and Fleagle, 1988: table 1). The angle between the axillary border of the scapula and the spine of the scapula (AS) is similar between the new specimen (30–32°) and MACN-SC 101 (30°). However, the AG and SG angles are much greater in the new specimen of *Homunculus*. From the photographs of MACN-SC 101, it appears that Anapol and Fleagle might have underestimated both AG and SG. It is clear from their fig. 2B that SG must be greater than 90° due to the lateral extension of the superior aspect of the glenoid (like the condition in the *Homunculus* specimen). It is also possible that the axillary border in the Pinturas specimen is partly broken away, leading to an underestimation of AG. Regardless of the condition in the Pinturas specimen, Anapol (1983) and Anapol and Fleagle (1988) suggested that pronograde primates have a very high AG angle (following Ashton and Oxnard, 1964). However, indriids have some of the greatest AG angles in their sample (as do cercopithecines). Indriids have a very low degree of pronogrady, so this feature is not a hallmark exclusive to horizontality of the trunk. It may be that the glenoid fossa of these Miocene platyrrhines bears a laterally extended superior part to brace the joint against superiorly directed loads. Such loads might occur

TABLE 7. Measurements of the scapula of MPM-PV 17453.

Measurement	Left Scapula	Right Scapula
Glenoid fossa height	12.03mm	11.93mm
Glenoid fossa width	7.60mm	7.69mm
Axillo-glenoid angle	138°	135°
Axillo-spinal angle	32°	30°
Spino-glenoid angle	106°	105°

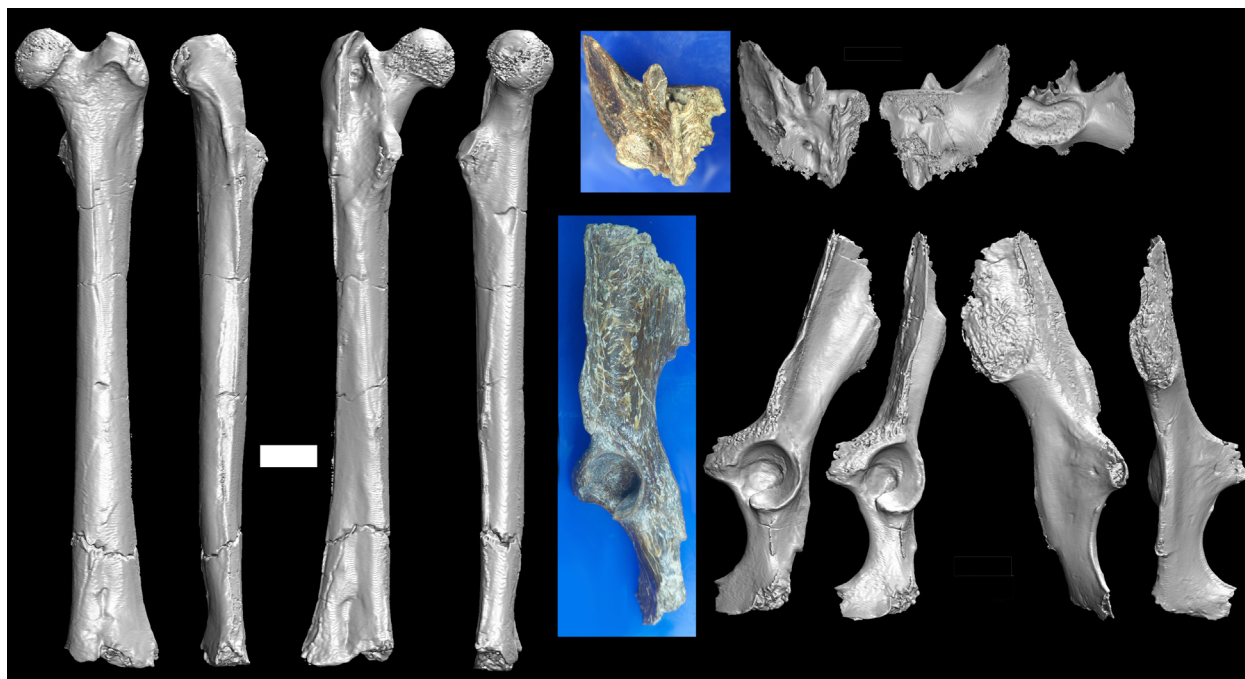


FIGURE 14. Femur, os coxa, and sacrum of *Homunculus patagonicus* MPM-PV 17453. Original photos are shown along with the CT surface reconstructions for the os coxa and sacrum. Scale bar equals 1 cm.

both in rapid terrestrial running with the head raised, and in heavy landings (after a leap) when the trunk is relatively upright. Given the lack of other morphological signals for terrestriality in *Homunculus*, this feature might indicate habitual forceful landings after leaps, with a relatively upright trunk. It is worth noting that this morphological feature is also seen in the scapula of *Apidium* (Anapol, 1983).

Femur. The left femur of MPM-PV 17453 is preserved from the proximal end down to the superior parts of the supracondylar ridges, likely 90% of its original length (Figure 14). The femur is strikingly like the complete right femur collected by Carlos Ameghino (MACN-A 5758). The association of MACN-A 5758 with a partial mandible (MACN-A 5757), the proposed neotype of *Homunculus patagonicus* (Tejedor and Rosenberger, 2008), is problematic (Bluntschli, 1931). MPM-PV 17453 is slightly more robust than MACN-A 5758 and has a slightly antero-posteriorly thicker greater trochanter. The amount of widening at the supracondylar ridges at the point of fracture suggests that the two femora were approximately the same length. The supero-inferior diameter of the femoral head of MPM-PV 17453 is slightly greater than that of MACN-A 5758 (13.0 mm versus 11.8 mm). The head of MPM-PV 17453 is spherical, perhaps slightly flattened in the disto-proximal axis; the

articular surface extends onto the upper and posterior side of the neck of the femur, as in MACN-A 5758. Ford (1990) noted this feature along with the high ridge medial to the trochanteric fossa in MACN-A 5758, which is also present in MPM-PV 17453. She suggested that this ridge is a strong insertion for obturator internus and cited the previous conclusion that the ridge and the continuation of the articular surface of the head onto the neck are features associated with leaping. Obturator internus is a lateral rotator of the hip, so emphasis of this muscle along with articular surface on the upper neck of the femur might be equally or more important for laterally rotating the thigh to reach distant supports when bridging from one branch to another in a sparse canopy. This is reinforced by the presence of these features in the suspensory atelines. The shaft of the femur is tubular, and the distal end is slightly broadened – but consistent with the relatively narrow distal articular end seen in MACN-A 5758.

Ciochon and Corruccini (1975) performed a principal components analysis of femoral dimensions in extant platyrrhines and *Homunculus*. They reported that the shape of the *Homunculus* femur most closely resembles that of the lion tamarin *Leontopithecus*. In the wild, the latter uses arboreal quadrupedalism and leaping locomotor equally to account for ~80% of its locomotion; vertical climb-

ing and suspensory locomotion are of limited importance (Stafford et al., 1996).

The morphology of the new femur reinforces conclusions drawn from the original one: namely, that *Homunculus* was a generalized arboreal quadruped. Evidence for some leaping behavior may still be present, especially in the form of the distal femur: the deep patellar groove in MACN-A 5758 might be a signal of the importance of leaping in this taxon (Ford, 1990).

Os Coxa. MPM-PV 17453 preserves the first pelvic bone known for *Homunculus*. It includes a complete acetabulum. Much of the iliac blade is intact (43 mm from acetabular rim to broken superior edge), and the anterior edge of the iliac crest is intact for about 6 mm, posterior to which it is broken away. The ischium is broken away just above the presumptive ischial tuberosity; it includes a small portion of the ischiopubic ramus; and the posterior rim is intact. The pubis is present only as a small bit of pubic crest. The lateral portion of the rim of the obturator foramen is intact.

The iliac blade in MPM-PV 17453 is long and somewhat broad compared to some platyrrhines (e.g., *Aotus*), similar in aspect ratio to some cercopithecine monkeys and quadrupedal lemurs. It is 43 mm long (supero-inferiorly) from the acetabular rim to the iliac crest and 21 mm at its broadest. The auricular surface is large, comprising about two-thirds of the width of the iliac blade, with some smooth surface anterior to it. The auricular surface is rugose, and the sacroiliac ligament was likely strong. The anterior inferior iliac spine is prominent and manifests as a long (11 mm) supero-inferior ridge. If the acetabulum is assumed to face directly laterally, then the outer (gluteal) surface of the iliac blade is oriented approximately half-way between the lateral plane and the dorsal plane.

The ischium is moderately thick at the acetabulum rim. It thickens markedly toward the ischial tuberosity and thins anteriorly. There is a distinct, but small, ischial spine. The ischial spine is noteworthy in being situated significantly below the inferior edge of the acetabulum rim (by ~9 mm). This suggests that the greater sciatic foramen was relatively large, perhaps for a well-developed piriformis muscle. The low position of the ischial spine also suggests that the obturator internus tendon had to turn quite sharply from its origin to course inferior to the low ischial spine and then turn sharply superiorly to reach the trochanteric fossa of the femur. This muscle would be stretched when the hip is extended and medially rotated but relaxed when it is flexed and laterally rotated.

The base of the pubis is thick and broad, with a rugose superior margin. The acetabulum is round and relatively shallow. The acetabular fossa is small relative to the lunate surface. There is a small bump for the anterior attachment of the transverse acetabular ligament, but no clear attachment feature for the posterior one. The superolateral portion of the acetabular rim, immediately inferior to the iliac blade, is smooth, essentially an interruption in the margin of the acetabulum. This smoothed-out portion of the acetabular rim directly faces the extension of articular bone onto the neck of the femur in highly abducted and somewhat medially rotated hip positions.

There is minor erosion of the articular surface of the femoral head. The femoral head fits easily inside the acetabulum, leaving little room between the articular surfaces. This is more like the condition in generalized arboreal quadrupeds than in suspensory platyrrhines like atelines, for example. Given the constraints imposed by muscles, tendons, and ligaments, the hip was probably habitually flexed as in most extant monkeys; for example, in greatly extended hip positions, the iliopsoas would be greatly stretched and twisted as the lesser trochanter is positioned quite far posteriorly. The conformity of the femoral head to the acetabulum suggests that stability was at a premium for the hip joint of *Homunculus*, perhaps sacrificing some mobility.

Sacrum. The sacrum is a rare find for a fossil platyrrhine. The later Miocene Colombian primate *Cebupithecia* has a fragmentary sacrum and a long series of caudal vertebrae (Organ and Lemelin, 2011); however, the new sacrum of *Homunculus* is the only other one known from a Miocene platyrrhine.

The sacrum of MPM-PV 17453 is broken, with only the majority of S1 and the cranial half of S2 present. There is a complete facet for the sacroiliac joint present on the left side. This alar surface matches the articulating auricular surface of the ilium precisely. The articulating surfaces are gently rugose, and the inferior end of the ilium is locked into articulation between this alar surface of the sacrum and the transverse process of the S2. The latter braces the ilium posteriorly. The superior surface of the S1 body is intact. The left superior articular process is complete, with complete facet, but the right one is broken away. This facet is nearly flat and oriented postero-medially, at about 45 degrees to the sagittal plane. An oblique breakage surface runs through the sacrum from the superolateral to inferomedial, and the right and inferior

portions of the sacrum are lost beyond that point. The sacral canal is sectioned through the inferior aspect of S2. The first anterior and posterior sacral foramina on the left are intact, but all other sacral foramina are lost.

The presence of a portion of sacral canal permits some exploration into tail length, as sacral canal ratios are indicators of tail length (Ankel, 1965). Sacral index (SI) is a ratio of sacral canal area (modeled as a square) at the caudal end of the sacrum relative to sacral canal area at the cranial end of the sacrum (Ankel, 1965; Russo, 2016). This can be calculated as $100 \times (\text{caudal breadth} \times \text{height}) / (\text{cranial breadth} \times \text{cranial height})$, where breadth is the maximum mediolateral dimension of the canal and height is the maximum dorsoventral dimension of the canal. Because the sacrum is broken away caudally, a very rough estimate of SI was made using sacral canal area at the point of breakage (near the caudal end of S2) as a stand-in for sacral canal area at the caudal end of the sacrum. This very likely overestimates SI because the sacrum tapers caudally in *Homunculus*. The proxy SI for *Homunculus* is 47.48 ($100 \times (2.90 \text{ mm} \times 1.68 \text{ mm}) / (4.04 \text{ mm} \times 2.54 \text{ mm})$). This value puts *Homunculus* in the range of non-prehensile short-tailed extant platyrrhines (Russo, 2016). Given that the caudal end of the sacral canal was undoubtedly even smaller in the complete sacrum of *Homunculus*, it is very likely that this extinct platyrrhine had a relatively short and certainly non-prehensile tail. Additional details of tail reconstruction must await a more complete sacrum.

Reconstruction of the Chewing Muscles

Physiological cross-sectional area (PCSA) for the three primary chewing muscle groups were reconstructed for *Homunculus patagonicus* using prediction equations from a sample of extant platyrrhines (Table 8). We found that the variation in both PCSA and muscle mass relative to osteological proxies made it difficult to predict these soft tissue variables with any confidence. Nevertheless, these results represent the best predictors of chewing muscle size currently available, and are, therefore, worth considering when reconstructing the paleobiology of *Homunculus*. The best predictors for PCSA were the origin areas for the temporalis and masseter, although the coefficients of determination for the reduced major axis regressions were only moderately high (0.566 and 0.459, respectively). Those for insertion areas were lower. The osteological proxies for medial pterygoid PCSA performed poorly (Table 8).

Proxies for muscle mass are determined as products of muscle attachment areas and the distance from the centroid of the origin area to the centroid of the insertion area. This approximated a 3D shape extending from one attachment area to the other. The most confident proxies (highest r-squared values for RMA regressions) were for insertion areas multiplied by the distance from centroid of origin to centroid of insertion, for temporalis and masseter. Again, these performed only modestly, while the proxies for medial pterygoid mass performed very poorly. The resulting masses for the temporalis, masseter, and medial pterygoid are

TABLE 8. Predicted values for *Homunculus* chewing muscle PCSA and mass.

Y var. (log)	X var. (log) ^a	RMA r-squared	LS slope	LS intercept	LS SEE ^b	LS QMLE ^c	<i>Homunculus</i> predicted ^d
Temporalis PCSA	TIA ^d	0.278	0.425	0.549	0.277	1.039	4.287
	TOA ^e	0.566	0.859	-0.393	0.215	1.023	2.649
Masseter PCSA	MIA ^f	0.369	0.738	0.353	0.215	1.023	5.860
	MOA ^g	0.459	0.940	1.064	0.327	1.055	3.345
MP PCSA	MPIA ^h	0.057	0.208	-0.097	0.328	1.055	0.928
	MPOA ⁱ	0.088	0.418	0.113	0.323	1.054	1.041
Temporalis Mass	TIA x To-ij	0.438	0.453	0.452	0.298	1.046	4.931
Masseter Mass	MIA x Mo-i	0.719	0.813	0.057	0.275	1.039	4.618
MPMass	MPIA x MPo-i	0.235	0.383	-0.392	0.351	1.064	0.643

^aSee Table 2 for explanation of abbreviations.

^bStandard Error of the Estimate (=Root Mean Square Error). See Perry et al. (2018) for explanation of prediction procedure.

^cQuasi-Maximum Likelihood Estimator. See Perry et al. (2018) for explanation of prediction procedure.

^dPredicted values for PCSA are in cm² and those for muscle volume are in g.

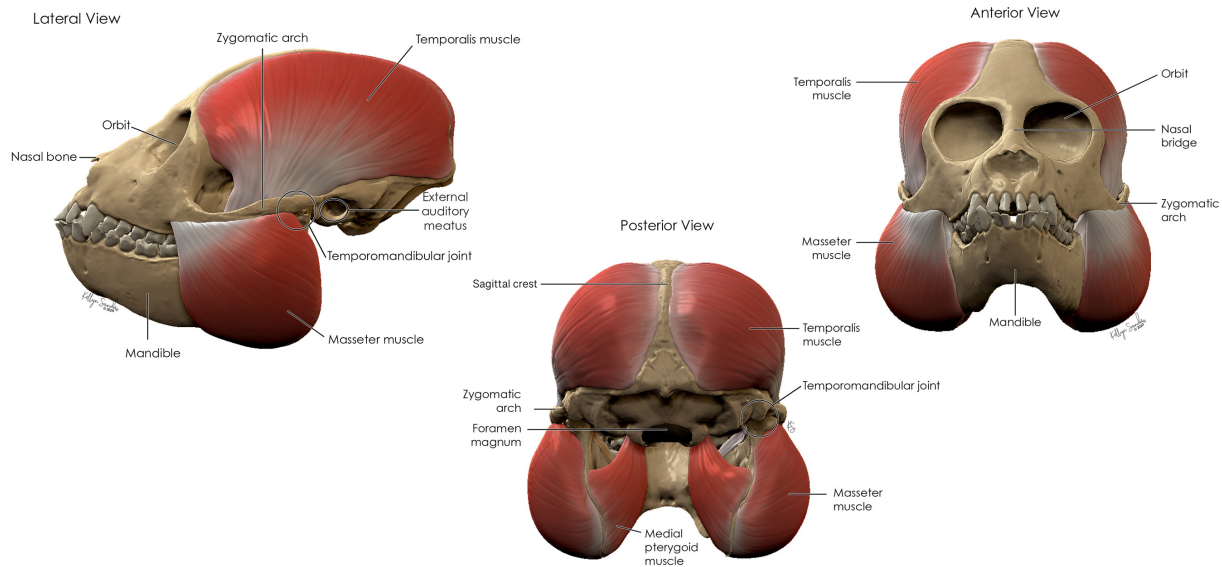


FIGURE 15. Reconstruction of chewing muscles of *Homunculus*.

4.9 g, 4.6 g, and 1.3 g, respectively (Table 8). These values were used to reconstruct the chewing muscles and layer them onto the restored skull model (Figure 15).

Poor proxies for the medial pterygoid are likely due to the extremely pinnate nature of this muscle, which consists of several sheets of short fibers bounded by aponeuroses. Thus, the area of bony attachment accommodates only a small percentage of the muscle fiber entheses.

The predicted physiological cross-sectional areas of the temporalis, masseter, and medial pterygoid muscles are shown in Table 8. These are the first such data from a specimen of *Homunculus* that has associated cranium and mandible; therefore, they are the first to contain no error from mixing of individuals. Figure 16 contextualizes the estimated PCSA of the temporalis and masseter of *Homunculus* among these values for extant platyrrhines (Table 9). Because the RMA for medial pterygoid had low explanatory value and thus low confidence in the regression-based estimate, results for this muscle are not shown. The position of *Homunculus* relative to the extant platyrrhines for PCSA suggests that this Miocene primate did not have especially forceful chewing muscles (Tauber, 1991; Perry et al., 2010); residuals are relatively small (-0.0365 for temporalis and 0.0497 for masseter). By contrast, residuals are somewhat large for both estimated temporalis mass (0.192) and masseter mass (0.234), and Figure 16 shows that the datum for *Homunculus* lies well above the least squares line of fit. This suggests that *Homun-*

culus had somewhat massive chewing muscles relative to head size among extant platyrrhines. Because muscle mass is reflective of both PCSA and fiber length, this suggests that *Homunculus* might have had somewhat long fibers compared to extant platyrrhines of similar head size. Generally, in primates, fiber length is an adaptation to gape and food size (Perry and Hartstone-Rose, 2010; Perry et al., 2015b); thus, *Homunculus* might have had a somewhat wide gape and ingested relatively large food items (fruits, seeds) compared to extant platyrrhines of similar head size. This is consistent with the observation that *Homunculus* had a relatively long snout compared to most extant platyrrhines (Perry et al., 2010).

The predicted volumes of chewing muscles were used to build a 3D model of the head of *Homunculus*. The resulting 3D object is a realistic restoration that is relatively complete, symmetrical, and that bears lifelike jaw adductor muscles (Figure 15). The predicted values for the temporalis and masseter were immediately recognized as lifelike in comparison to dissections of extant platyrrhines of similar size. However, the value for the medial pterygoid (which had been calculated from the proportion of medial pterygoid mass to that of temporalis and masseter) was found to be unrealistically small. When an attempt was made to stretch this volume from the origin to the insertion on the skull model, this produced an absurdly thin muscle belly. Doubling the volume yielded a much more realistic muscle model and this was used in the final reconstruction. The fact that this value

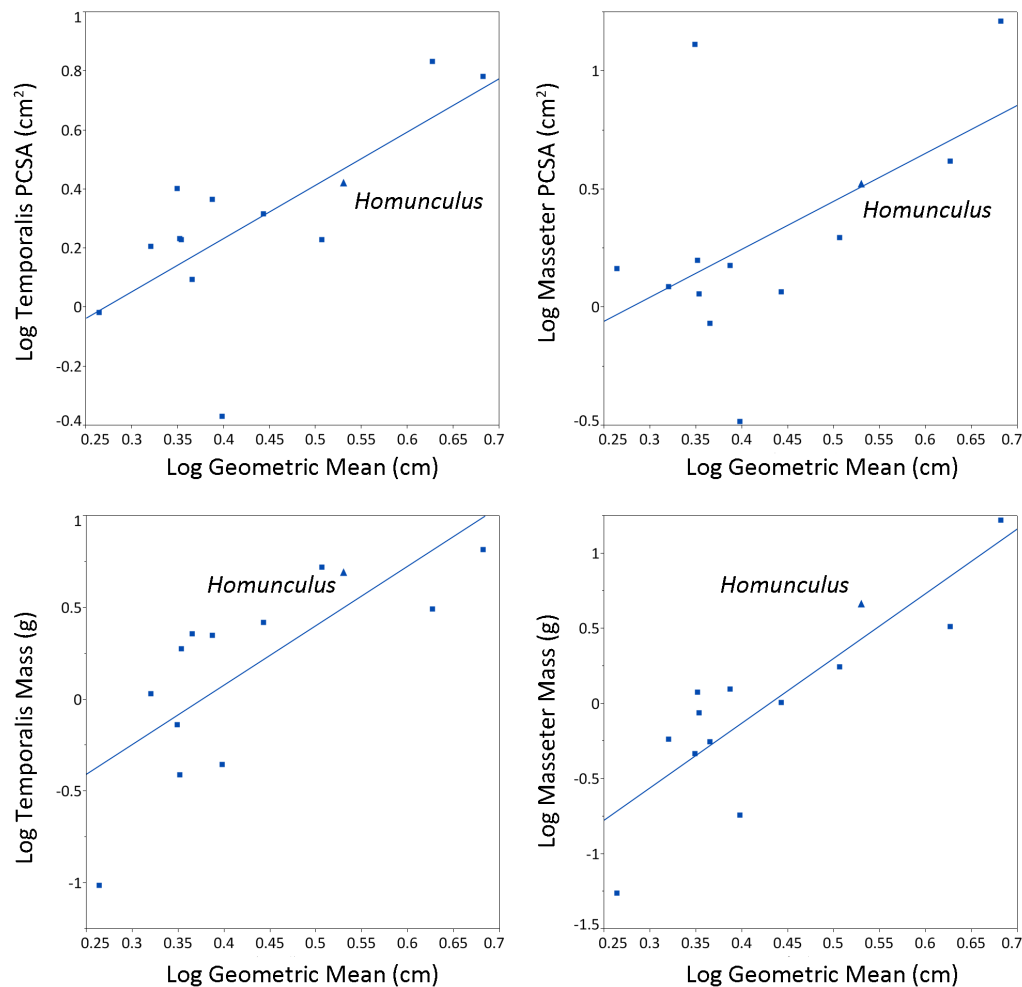


FIGURE 16. Least squares plots of temporalis and masseter PCSA and mass against a geometric mean of nine skull measurements. For measurements, see Table 8. The datum for *Homunculus* is shown by a cross. See text for details.

needed to be doubled to produce a realistic image suggests that the medial pterygoid muscle in *Homunculus* might have been proportionately large relative to the temporalis and masseter (as compared to extant platyrrhines of like size) and severely underestimated by the regression prediction for its mass from osteological traits. This trait (a large medial pterygoid relative to other jaw adductors muscles) is also observed in some extant strepsirrhines and platyrrhines but is more typically seen in herbivorous species that are more folivorous than frugivorous.

DISCUSSION AND CONCLUSIONS

Homunculus patagonicus MPM-PV 17453 is the most complete and well-preserved specimen of a primate from the Miocene of South America. It preserves several key elements in association, including a cranium, mandible, nearly all the teeth,

temporomandibular joints, upper and lower limb elements, a glenohumeral joint, a hip joint, and a sacroiliac joint. Its completeness and preservation permit unprecedented testing of anatomical and biomechanical hypotheses in the taxon that reached the southern-most latitudinal geographic range of any monkey species. The presence of a complete skull in association reinforces the conclusion that *Homunculus* had relatively large chewing muscles, even if the exact sizes of these are difficult to infer from bony features alone. These muscles were large perhaps more due to the need for attaining a wide gape than a disproportionate need for force, suggesting medium-large objects in the diet. Cheek teeth show signs of significant wear in most specimens, including MPM-PV 17453; this suggests an abrasive diet, consistent with periodic influx of tuffaceous soil onto the foods of *Homunculus* (see Madden, 2015). Although somewhat dis-

TABLE 9. Dimensions of chewing muscles for extant platyrrhines and those estimated for *Homunculus*.

Species	Log GM (cm) ^a	Temporalis		Masseter		Medial Pterygoid	
		Log PCSA (cm ²)	Log Mass (g)	Log PCSA (cm ²)	Log Mass (g)	Log PCSA (cm ²)	Log Mass (g)
<i>Aotus nancymaae</i>	0.506	0.230	0.721	0.297	0.247	-0.335	-0.674
<i>Callithrix jacchus</i>	0.354	0.230	0.278	0.059	-0.059	-0.121	-0.509
<i>Callithrix pygmaea</i>	0.264	-0.018	-1.012	0.166	-1.261	-0.111	-2.234
<i>Chiropotes sagulatus</i>	0.682	0.783	0.816	1.213	1.222	0.303	0.217
<i>Mico argentatus</i>	0.320	0.207	0.031	0.089	-0.234	-0.359	-0.757
<i>Saguinus imperator</i>	0.352	0.233	-0.409	0.199	0.079	-0.389	-0.620
<i>Saguinus labiatus</i>	0.387	0.366	0.350	0.178	0.097	-0.210	-0.347
<i>Saguinus midas</i>	0.398	-0.368	-0.353	-0.482	-0.740	-0.645	-1.081
<i>Saguinus oedipus</i>	0.365	0.096	0.358	-0.066	-0.252	-0.263	-0.538
<i>Saimiri sciureus</i>	0.443	0.318	0.420	0.066	0.009	-0.037	-0.222
<i>Sapajus apella</i>	0.627	0.833	0.494	0.621	0.513	0.478	0.222
<i>Homunculus patagonicus</i>	0.530	0.423	0.693	0.524	0.664	n/a	n/a

^aThe geometric mean is composed of the following measurements: mandible length, cranial length, corpus height below m2, maximum skull height in articulation, max orbit height, max bizygomatic breadth, cranial breadth behind zygomatic arches, breadth at the postorbital constriction, max bi-orbital breadth.

tant from active volcanoes themselves, the habitat of *Homunculus* was “downstream” of volcanic areas and probably experienced frequent dust storms that coated trees with abrasive material. The new specimen reinforces inferences drawn from other cranial specimens that *Homunculus* fed on fruits, leaves, and seeds, including resistant items of a relatively large size for its mouth. Many of these foods would have contained abrasive phytoliths and/or been covered in soil or dust of an abrasive nature. Additionally, even if it was predominantly a frugivore in seasons of abundance, being at such a high latitude would have precluded frugivory year-around (Li et al., 2020). Temperature seasonality is highly correlated with latitude, leading to strong seasonality of fruit production. Even a committed non-volant mammalian frugivore cannot find fruit at some times of the year (Kay et al. 2021).

The postcranial elements of MPM-PV 17453 provide evidence for posture and locomotion in *Homunculus*. The overall picture is one of a generalized arboreal quadruped. However, the glenohumeral joint suggests adaptations for considerable shoulder extension, and the scapula suggests that the shoulder was adapted to withstanding compressive loads at the superior margin of the glenoid fossa. The femur and os pelvis suggest that the hip was adapted to flexed postures and wide abduction. This is consistent with an animal that climbed large diameter vertical supports, bridged large

gaps in the canopy, and leaped from one support to another habitually—as does *Leontopithecus* today. As temperature and humidity in Patagonia decreased towards the end of the Middle Miocene Climatic Optimum, it is likely that forest canopies thinned out and gaps between suitable supports for a small monkey grew. Although speculative, *Homunculus* might have adopted multiple strategies to move from one tree to another, including terrestrial locomotion, bridging, and leaping. This would have necessitated frequent ascending and descending of large diameter vertical supports.

Previous estimates of body mass for *Homunculus patagonicus* represent a broad range of values depending on the element used for the estimate and on the extant reference sample (see Perry et al., 2018; Fleagle et al., 2022. MPM-PV 17453 has well preserved, relatively complete long bones, which yield new body mass estimates (average from humerus and femur = 2,164 g). *Homunculus* was a small-to-medium sized platyrrhine, in the size range of a titi monkey (*Callicebus*) or a saki monkey (*Pithecia*).

The above paleobiological inferences should be regarded as preliminary in some cases as considerable analysis remains to be done on the skeleton. For example, joint excursions are estimated in only a qualitative fashion here. Additional studies of the joints, including bone microstructure, might reveal additional biomechanical patterns. Equally lacking is information about the distal extremities;

the hand/wrist and foot/ankle of *Homunculus* remain completely unknown.

Whereas the paleobiology of *Homunculus* still has many unanswered questions, one fact is now quite certain: the specimens previously described as *Homunculus patagonicus* and those described as *Killikaike blakei* all belong to a single species with some limited intraspecific variation. The presence of associated upper and lower dentition puts to rest any uncertainty about the attribution of cranial and mandibular specimens.

Homunculus patagonicus was an herbivorous, diurnal, generalized quadruped. It fed on tough, possibly gritty foods, ingested at somewhat large volumes. It spent time climbing vertical tree trunks and crossing large gaps in the canopy by bridging, leaping, and probably sometimes descending to the forest floor. It lived prior to a time of cooling and aridification that ultimately led, in all probability, to the extinction of its descendants. *Homunculus* was one of a handful of early platyrrhines that radiated in the early Miocene and dispersed to high latitudes, all of which became extinct as temperatures and rainfall dropped (Kay, 2015). Several of its cra-

nial and postcranial features may have been adaptations to this environment in collapse.

ACKNOWLEDGMENTS

We thank all the Duke University-Museo de La Plata field crews from 2002 to the present day, especially the 2015 field crew. We thank the Dirección de Patrimonio, Secretaría de Cultura de Estado (Santa Cruz Province), and Museo Regional Provincial Padre M.J. Molina. We thank J. Battini and his family for their kindness and for providing accommodations at Estancia La Costa for many seasons. Thanks to M. Malinzak for completing the virtual endocast of MPM-PV 3502. Thanks to N. Utrup for scanning and providing the original that appears here as Figure 1. We are grateful to two anonymous reviewers and the editorial staff who provided substantial improvements to this paper. Funding for this work was graciously provided by National Science Foundation grant BCS 1749307 / 2203690, an American Association for Anatomy Fellows Grant, as well as by PICT 2013-0389, 2017-1081, UNLP N867, and UNLP N997.

REFERENCES

- Ameghino, F. 1891a. Nuevos restos de mamíferos fósiles descubiertos por C. Ameghino en el Eoceno inferior de la Patagonia austral. Especies nuevas, adiciones y correcciones. *Revista Argentina de Historia Natural*, 1:289–328.
- Ameghino, F. 1891b. Los monos fósiles del eoceno de la República Argentina. *Revista Argentina de Historia Natural*, 1:383–397.
- Ameghino, F. 1898. Sinopsis geológico-paleontológica de la Argentina. Segundo Censo de la República Argentina, 1:112–255.
- Anapol, F. 1983. Scapula of *Apidium phiomense*: A small anthropoid from the Oligocene of Egypt. *Folia Primatologica*, 40:11–31.
<https://doi.org/10.1159/000156089>
- Anapol, F. and Fleagle, J.G. 1988. Fossil platyrrhine forelimb bones from the early Miocene of Argentina. *American Journal of Physical Anthropology*, 76:417–428.
<https://doi.org/10.1002/ajpa.1330760402>
- Ankel, F. 1965. Der Canalis sacralis als Indikator für die Länge der Caudalregion der Primaten. *Folia Primatologica*, 3:263–276.
<https://doi.org/10.1159/000155038>
- Ashton, E.H. and Oxnard, C.E. 1964. Functional adaptations in the primate shoulder girdle. *Proceedings of the Zoological Society of London*, 142:49–66.
<https://doi.org/10.1111/j.1469-7998.1964.tb05153.x>
- Beck, R.M.D., de Vries, D., Janiak, M.C., Goodhead, I.B., and Boubli, J.P. 2023. Total evidence phylogeny of platyrrhine primates and a comparison of undated and tip-dating approaches. *Journal of Human Evolution*, 174:103293.
<https://doi.org/10.1016/j.jhevol.2022.103293>
- Bluntshli, H. 1913. Die fossilen Affen Patagoniens und der Ursprung der platyrrhinen Affen. *Verhandlungen der anatomischen Gesellschaft*, 27:33–43.

- Bluntschli, H. 1931. *Homunculus patagonicus* und die ihm zugereichten Fossilfunde aus den Santa-Cruz-Schichten Patagoniens. *Morphologisches Jahrbuch*, 67:811–892.
- Bordas, A.F. 1942. Anotaciones sobre un 'Cebidae' fosil de Patagonia. *Physis*, 19:265–269.
- Bush, E.C., Simons, E.L., and Allman, J. 2003. Brain anatomy of *Parapithecus grangeri*, p. 587–598. In Ross, C. and Kay, R.F. (ed.), *Anthropoid Origins: New Visions*. Kluwer/Plenum Publishing, New York.
- Bush, E.C., Simons, E.L. and Allman, J. 2004. High-resolution computed tomography study of the cranium of a fossil anthropoid primate, *Parapithecus grangeri*: New insights into the evolutionary history of primate sensory systems. *Anatomical Record, Part A* 281A:1083–1087.
<https://doi.org/10.1002/ar.a.20113>
- Cartmill, M. and Kay, R.F. 1978. Craniodental morphology, tarsier affinities, and primate suborders, p. 205–214. In Chivers, D.J. and Joysey, K.A. (ed.), *Recent Advances in Primatology: Evolution*. Academic Press, London.
- Cartmill, M., Mac Phee, R.D.E. and Simons, E.L. 1981. Anatomy of the temporal bone in early anthropoids with remarks on the problem of anthropoid origins. *American Journal of Physical Anthropology*, 56:3–21.
<https://doi.org/10.1002/ajpa.1330560102>
- Ciochon, R.L. and Corruccini, R.S. 1975. Morphometric analysis of platyrrhine femora with taxonomic implications and notes on two fossil forms. *Journal of Human Evolution*, 4:193–217.
[https://doi.org/10.1016/0047-2484\(75\)90008-1](https://doi.org/10.1016/0047-2484(75)90008-1)
- Conroy, G. 1980. Evolutionary significance of cerebral venous patterns in paleoprimatology. *Zeitschrift für Morphologie und Anthropologie*, 71:125–134.
<https://doi.org/10.1127/zma/71/1980/125>
- Cooke, S.B., Gladman, J.T., Halenar, L.B., Klukkert, Z.S., and Rosenberber, A.L. 2016. The paleobiology of the recently extinct platyrrhines of Brazil and the Caribbean, p. 41–89. In Ruiz, M. (ed.), *Molecular Population Genetics, Evolutionary Biology and Biological Conservation of Neotropical Primates*. Nova Publishers, New York.
- Cuitiño, J.I., Fernicola, J.C., Kohn, M.J., Trayler, R., Naipauer, M., Bargo, M.S., Kay, R.F., and Vizcaíno, S. F. 2016. U-Pb geochronology of the Santa Cruz Formation (early Miocene) at the Río Bote and Río Santa Cruz (southernmost Patagonia, Argentina): Implications for the correlation of fossil vertebrate localities. *Journal of South American Earth Sciences*, 70:198–210.
<https://doi.org/10.1016/j.jsames.2016.05.007>
- Cuitiño, J.I., Raigemborn, M.S., Bargo, M.S., Vizcaíno, S.F., Muñoz, N.A., Kohn, M.J., and Kay, R.F. 2021. Insights on the controls on floodplain-dominated fluvial successions: a perspective from the early-middle Miocene Santa Cruz Formation in Río Chalfá (Patagonia, Argentina). *Journal of the Geological Society*, 178:jgs2020–188.
<https://doi.org/10.1144/jgs2020-188>
- Deutsch, A.R., Dickinson, E., Leonard, K.C., Pastor, F., Muchlinski, M.N., and Hartstone-Rose, A. 2020. Scaling of anatomically derived maximal bite force in primates. *The Anatomical Record*, 303:2026–2035.
<https://doi.org/10.1002/ar.24284>
- Dickinson, E., Stark, H., and Kupczik, K. 2018. Non-destructive determination of muscle architectural variables through the use of DiceCT. *The Anatomical Record*, 301:363–377.
<https://doi.org/10.1002/ar.23716>
- Dickinson, E., Pastor, F., Santana, S.E., and Hartstone-Rose, A. 2022. Functional and ecological correlates of the primate jaw abductors. *The Anatomical Record*, 305:1245–1263.
<https://doi.org/10.1002/ar.24772>
- Fleagle, J.G. 1990. New fossil platyrrhines from the Pinturas Formation, southern Argentina. *Journal of Human Evolution*, 19:61–85.
[https://doi.org/10.1016/0047-2484\(90\)90012-Z](https://doi.org/10.1016/0047-2484(90)90012-Z)
- Fleagle, J.G. and Simons, E.L. 1982. The humerus of *Aegyptopithecus zeuxis*: a primitive anthropoid. *American Journal of Physical Anthropology*, 59:175–193.
<https://doi.org/10.1002/ajpa.1330590207>
- Fleagle, J.G. and Simons, E.L. 1982. Skeletal remains of *Propliopithecus chirobates* from the Egyptian Oligocene. *Folia Primatologica*, 39:161–177.
<https://doi.org/10.1159/000156075>

- Fleagle, J.G. and Kay, R.F. 1983. New interpretations of the phyletic position of Oligocene hominoids, p. 181–210. In Ciochon, R.L. and Corruccini, R.S. (ed.), *New Interpretations of Ape and Human Ancestry*. Plenum Press, New York and London.
https://doi.org/10.1007/978-1-4684-8854-8_7
- Fleagle, J.G. and Rosenberger, A.L. 1983. Cranial morphology of the earliest anthropoids, p. 141–155. In Sakka, M. (ed.), *Morphologie Evolution Morphogenese du Crane et Origine de l'Homme*. Centre National de Recherche Scientifique, Paris.
- Fleagle, J.G. and Kay, R. F. 1987. The phyletic position of the Parapithecidae. *Journal of Human Evolution*, 16:483–532.
[https://doi.org/10.1016/0047-2484\(87\)90036-4](https://doi.org/10.1016/0047-2484(87)90036-4)
- Fleagle, J.G., Powers, D.W., Conroy, G.C., and Watters, J.P. 1987. New fossil platyrrhines from Santa Cruz Province, Argentina. *Folia Primatologica*, 48:65–77.
<https://doi.org/10.1159/000156286>
- Fleagle, J.G., Buckley, G.A., and Schloeder, M.E. 1988. New primate fossils from Monte Observación, Santa Cruz Formation (lower Miocene), Santa Cruz Province, Argentina. *Journal of Vertebrate Paleontology*, 8:14A.
- Fleagle, J.G. and Meldrum, D.J. 1988. Locomotor behavior and skeletal morphology of two sympatric pitheciine monkeys, *Pithecia pithecia* and *Chiropotes satanas*. *American Journal of Primatology*, 16:227-249.
<https://doi.org/10.1002/ajp.1350160305>
- Fleagle, J.G. and Simons, E.L. 1995. Limb skeleton and locomotor adaptations of *Apidium phiomense*, an Oligocene anthropoid from Egypt. *American Journal of Physical Anthropology*, 97:235–289.
<https://doi.org/10.1002/ajpa.1330970303>
- Fleagle, J.G., Perkins, M.E., Heizler, M.T., Nash, B., Bown, T.M., Tauber, A.A., Dozo, M.T., and Tejedor, M.F. 2012. Absolute and relative ages of fossil localities in the Santa Cruz and Pinturas Formations, p. 41–58. In Vizcaíno, S.F., Kay, R.F., and Bargo, M.S. (ed.), *Early Miocene Paleobiology in Patagonia: High-Latitude Paleocommunities of the Santa Cruz Formation*. Cambridge University Press, Cambridge.
<https://doi.org/10.1017/cbo9780511667381.004>
- Fleagle, J.G. and Lieberman, D.E. 2015. Major transformations in the evolution of primate locomotion, p. 257–278. In Dial, K.P., Shubin, N., and Brainerd, E.L. (ed.), *Great Transformations in Vertebrate Evolution*. University of Chicago Press, Chicago, IL.
<https://doi.org/10.7208/chicago/9780226268392.003.0015>
- Fleagle, J.G., Gladman, J.T., and Kay, R.F. 2022. A new humerus of *Homunculus patagonicus*, a stem platyrrhine from the Santa Cruz Formation (Late Early Miocene), Santa Cruz Province, Argentina. *Ameghiniana*, 59:78–97.
<https://doi.org/10.5710/AMGH.29.09.2021.3447>
- Flynn, J.J., Wyss, A.R., Charrier, R., and Swisher, C.C.I. 1995. An early Miocene anthropoid skull from the Chilean Andes. *Nature*, 373:603–607.
<https://doi.org/10.1038/375253c0>
- Ford, S. M. 1990. Locomotor adaptations of fossil platyrrhines. *Journal of Human Evolution*, 19:141–173.
<https://doi.org/10.1016/B978-0-12-260345-7.50010-2>
- Fulwood, E.L., Boyer, D.M., and Kay, R.F. 2016. Stem members of Platyrrhini are distinct from catarrhines in at least one derived cranial feature. *Journal of Human Evolution*, 100:16–24.
<https://doi.org/10.1016/j.jhevol.2016.08.001>
- Garland, T. Jr. and Ives, A.R. 2000. Using the past to predict the present: confidence intervals for regression equations in phylogenetic comparative methods. *The American Naturalist*, 155:346–364.
<https://doi.org/10.1086/303327>
- Hartstone-Rose, A., Deutsch, A. R., Leischner, C.L., and Pastor, F. 2018. Dietary correlates of primate masticatory muscle fiber architecture. *The Anatomical Record*, 301:311–324.
<https://doi.org/10.1002/ar.23715>
- Heesy, C.P. 2003. The evolution of orbit orientation in mammals and the function of the primate postorbital bar. PhD Thesis, Stony Brook University, Stony Brook, NY.
- Hershkovitz, P. 1974. A new genus of Late Oligocene monkey (Cebidae, Platyrrhini) with notes on postorbital closure and platyrrhine evolution. *Folia Primatologica*, 21:1-35.
<https://doi.org/10.1159/000155594>

- Hershkovitz, P. 1977. Living New World monkeys (Platyrrhini) with an introduction to Primates, Vol. 1. University of Chicago Press, Chicago.
- Hershkovitz, P. 1982. Supposed squirrel monkey affinities of the late Oligocene *Dolichocebus gaimanensis*. *Nature*, 298:201–202.
<https://doi.org/10.1038/298201a0>
- Horovitz, I. 1997. Platyrrhine systematics and the origin of Greater Antilles monkeys. PhD Thesis, State University of New York, Stony Brook, NY.
- Horovitz, I. 1999. A phylogenetic study of living and fossil platyrrhines. *American Museum Novitates*. New York NY, 3269:1–40.
- Horovitz, I. and MacPhee, R.D.E. 1999. The Quaternary Cuban platyrrhine *Paralouatta varonai* and the origin of Antillean monkeys. *Journal of Human Evolution*, 36:33–68.
<https://doi.org/10.1006/jhev.1998.0259>
- Kay, R.F. 2010. A new primate from the Early Miocene of Gran Barranca, Chubut Province, Argentina: paleoecological implications, p. 220–239. In Madden, R.H., Vucetich, G., Carlini, A.A. and Kay, R.F. (ed.), *The Paleontology of Gran Barranca: Evolution and Environmental Change through the Middle Cenozoic of Patagonia*. Cambridge University Press, Cambridge.
- Kay, R.F. 2015. Biogeography in deep time—What do phylogenetics, geology, and paleoclimate tell us about early platyrrhine evolution? *Molecular Phylogenetics and Evolution*, 82:358–374.
<https://doi.org/10.1016/j.ympev.2013.12.002>
- Kay, R.F. and Fleagle, J.G. 2010. Stem taxa, homoplasy, long lineages and the phylogenetic position of *Dolichocebus*. *Journal of Human Evolution*, 59:218–222.
<https://doi.org/10.1016/j.jhevol.2010.03.002>
- Kay, R.F. and Perry, J.M.G. 2019. New primates from the Río Santa Cruz and Río Bote (early-Middle Miocene), Santa Cruz Province, Argentina. *Publicación Electrónica de la Asociación Paleontológica Argentina*, 19:230–238.
<https://doi.org/10.5710/PEAPA.24.08.2019.289>
- Kay, R.F., Campbell, V.M., Rossie, J.B., Colbert, M.W., and Rowe, T.B. 2004. Olfactory fossa of *Tremacebus harringtoni* (Platyrrhini, Early Miocene, Sacanana, Argentina): implications for activity pattern. *The Anatomical Record Part A*, 281A:1157–1172.
<https://doi.org/10.1002/ar.a.20121>
- Kay, R.F., Fleagle, J.G., Mitchell, T.R.T., Colbert, M.W., Bown, T.M., and Powers, D.W. 2008a. The anatomy of *Dolichocebus gaimanensis*, a stem platyrrhine monkey from Argentina. *Journal of Human Evolution*, 54, 3:323–382.
<https://doi.org/10.1016/j.jhevol.2007.09.002>
- Kay, R.F., Simons, E.L., and Ross, J.L. 2008b. The basicranial anatomy of African Eocene/Oligocene anthropoids. Are there any clues for platyrrhine origins?, p. 125–158. In Fleagle, J.G. and Gilbert, C.G. (ed.), *Elwyn L. Simons: A Search for Origins*. Springer, New York.
https://doi.org/10.1007/978-0-387-73896-3_11
- Kay, R.F., Perry, J.M.G., Malinzak, M., Allen, K.L., Kirk, E., Plavcan, J.M., and Fleagle, J.G. 2012. Paleobiology of Santacrucian primates, p. 306–330. In Vizcaíno, S.F., Kay, R.F., and Bargo, M. S. (ed.), *Early Miocene Paleobiology in Patagonia: High-Latitude Paleocommunities of the Santa Cruz Formation*. Cambridge University Press, Cambridge.
<https://doi.org/10.1017/cbo9780511667381.017>
- Kay, R.F., Vizcaíno, S.F., Bargo, M.S., Spradley, J.P. and Cuitiño, J.I. 2021. Paleoenvironments and paleoecology of the Santa Cruz Formation (early-middle Miocene) along the Río Santa Cruz, Patagonia (Argentina). *Journal of South American Earth Sciences*, 109:103296.
<https://doi.org/10.1016/j.jsames.2021.103296>
- Kraglievich, J. L. 1951. Contribuciones al conocimiento de los primates fosiles de la Patagonia. I. Diagnósis previa de un nuevo primat fosil del Oligoceno superior (Colheuhupiano) de Gaiman, Chubut. *Comunicaciones del Instituto Nacional de Investigaciones de las Ciencias Naturales*, II, Ciencias Zoológica, 11:57–82.
- Li, P., Morse, P.E., and Kay, R.F. 2020. Dental topographic change with macrowear and dietary inference in *Homunculus patagonicus*. *Journal of Human Evolution*, 144:102786.
<https://doi.org/10.1016/j.jhevol.2020.102786>
- Lundeen, I.K. and Kay, R.F. 2022. Unique nasal turbinal morphology reveals *Homunculus patagonicus* functionally converged on modern platyrrhine olfactory sensitivity. *Journal of Human Evolution*, 167:103184.
<https://doi.org/10.1016/j.jhevol.2022.103184>

- MacPhee, R.D.E. and Cartmill, M. 1986. Basicranial structures and primate systematics, p. 219–275. In Swindler, D.R. and Erwin, J. (ed.), *Comparative Primate Biology, Volume 1: Systematics, Evolution, and Anatomy*. Alan R. Liss, New York.
- MacPhee, R.D.E., Horovitz, I., Arredondo, O., and Jiménez Vázquez, O. 1995. A new genus for the extinct Hispaniolan monkey *Saimiri bernensis* Rímoli, 1977, with notes on its systematic position. *American Museum Novitates*. New York NY, 3134:1–21.
- Madden, R.H. 2015. *Hypsodonty in Mammals: Evolution, Geomorphology, and the Role of Earth Surface Processes*. Cambridge University Press, Cambridge.
<https://doi.org/10.1017/CBO9781139003384> **[AUTHOR DOI says 2014 but you list 2015]**
- Matheos, S.D. and Raigemborn, M.S. 2012. Sedimentology and paleoenvironment of the Santa Cruz Formation, p. 59–82. In Vizcaíno, S.F., Kay, R.F. and Bargo, M.S. (ed.), *Early Miocene Paleobiology in Patagonia: High-Latitude Paleocommunities of the Santa Cruz Formation*. Cambridge University Press, Cambridge.
<https://doi.org/10.1017/CBO9780511667381.005>
- Meldrum, D.J. and Fleagle, J.G. 1988. Morphological affinities of the postcranial skeleton of *Cebupithecia sarmientoi*. *American Journal of Physical Anthropology*, 75:249–250.
- Meldrum, D.J. and Kay, R.F. 1990. A new partial skeleton of *Cebupithecia sarmientoi* from the Miocene of Colombia. *American Journal of Physical Anthropology*, 81:267.
- Meldrum, D.J., Fleagle, J.G., and Kay, R.F. 1990. Partial humeri of two Miocene Colombian primates. *American Journal of Physical Anthropology*, 81:413–422.
<https://doi.org/10.1002/ajpa.1330810310>
- Mercerat, A. 1891. Sobre la presencia de restos de monos en el eoceno de Patagonia. *Revista del Museo de La Plata*, 2:73–74.
- Ni, X., Flynn, J.J., Wyss, A.R., and Zhang, C., 2019. Cranial endocast of a stem platyrrhine primate and ancestral brain conditions in anthropoids. *Science Advances*, 5:eaav7913.
<https://doi.org/10.1126/sciadv.aav7913>
- Novo, N.M., Tejedor, M.F., Gonzalez-Ruiz, L.R., Fleagle, J.G., Brandoni, D., and Krause, M. 2021. Primate diversity in the early Miocene Pinturas Formation, southern Patagonia, Argentina. *Anais da Academia Brasileira de Ciências*, 93:10.1590/0001-3765202120201218
<https://doi.org/10.1590/0001-3765202120201218>
- Nunn, C.L. and Zhu, L. 2014. Phylogenetic prediction to identify “evolutionary singularities”, p. 482–514. In Garamszegi, L. (ed.), *Modern Phylogenetic Comparative Methods and Their Application in Evolutionary Biology*. Springer, Berlin, Heidelberg.
https://doi.org/10.1007/978-3-662-43550-2_21
- Organ, J.M. and Lemelin, P. 2011. Tail architecture and function of *Cebupithecia sarmientoi*, a Middle Miocene platyrrhine from La Venta, Colombia. *The Anatomical Record*, 294:2013–2023.
<https://doi.org/10.1002/ar.21504>
- Pampush, J.D., Fuselier, E.J., and Yapuncich, G.S. 2021. Using BayesModelS to provide Bayesian-and phylogenetically-informed primate body mass predictions. *Journal of Human Evolution*, 161:103077.
<https://doi.org/10.1016/j.jhevol.2021.103077>
- Perkins, M.E., Fleagle, J.G., Heizler, M.T., Nash, B., Bown, T.M., Tauber, A.A., and Dozo, M.T. 2012. Tephrochronology of the Miocene Santa Cruz and Pinturas Formations, Argentina, p. 23–40. In Vizcaíno, S.F., Kay, R.F., and Bargo, M.S. (ed.), *Early Miocene Paleobiology in Patagonia: High-Latitude Paleocommunities of the Santa Cruz Formation*. Cambridge University Press, Cambridge.
<https://doi.org/10.1017/CBO9780511667381.003>
- Perry, J.M.G. 2018. Inferring the diets of extinct giant lemurs from osteological correlates of muscle dimensions. *The Anatomical Record*, 301:343–362.
<https://doi.org/10.1002/ar.23719>
- Perry, J.M.G. and Hartstone-Rose, A. 2010. Maximum ingested food size in captive strepsirrhine primates: scaling and the effects of diet. *American Journal of Physical Anthropology*, 142:625–635.
<https://doi.org/10.1002/ajpa.21285>
- Perry, J.M.G., Kay, R.F., Vizcaíno, S.F., and Bargo, M.S. 2010. Tooth root size, chewing muscle leverage, and the biology of *Homunculus patagonicus* (Primates) from the late early Miocene of Patagonia. *Ameghiniana*, 47:355–371.
<https://doi.org/10.5710/AMGH.v47i3.9>

- Perry, J.M.G., Kay, R.F., Vizcaíno, S.F., and Bargo, M.S. 2014. Oldest known cranium of a juvenile New World monkey (Early Miocene, Patagonia, Argentina): implications for the taxonomy and the molar eruption pattern of early platyrrhines. *Journal of Human Evolution*, 74:67–81.
<https://doi.org/10.1016/j.jhevol.2014.03.009>
- Perry, J.M.G., St Clair, E.M., and Hartstone-Rose, A. 2015a. Craniomandibular signals of diet in adapids. *American Journal of Physical Anthropology*, 158:646–662.
<https://doi.org/10.1002/ajpa.22811>
- Perry, J.M.G., Bastian, M.L., St Clair, E.M., and Hartstone-Rose, A. 2015b. Maximum ingested food size in captive anthropoids. *American Journal of Physical Anthropology*, 158:92–104.
<https://doi.org/10.1002/ajpa.22779>
- Perry, J.M.G., Cooke, S.B., Runestad Connour, J.A., Burgess, M.L., and Ruff, C.B. 2018. Articular scaling and body mass estimation in platyrrhines and catarrhines: Modern variation and application to fossil anthropoids. *Journal of Human Evolution*, 115:20–35.
<https://doi.org/10.1016/j.jhevol.2017.10.008>
- R Core Team. 2022. R: A Language and Environment for Statistical Computing. R Foundation for Statistical Computing, Vienna, Austria.
- Rosenberger, A.L. 1979a. Cranial anatomy and implications of *Dolichocebus*, a late Oligocene ceboid primate. *Nature*, 279:416–418.
<https://doi.org/10.1038/279416a0>
- Rosenberger, A.L. 1979b. Phylogeny, evolution and classification of New World monkeys (Platyrrhini, Primates). PhD Thesis, City University of New York, New York, NY.
- Rosenberger, A.L. 1982. Supposed squirrel monkey affinities of the late Oligocene *Dolichocebus gaimanensis*, reply to P. Hershkovitz. *Nature*, 298:202.
<https://doi.org/10.1038/298202a0>
- Rosenberger, A.L. 1985. In favor of the *Necrolemur-Tarsius* hypothesis. *Folia Primatologica*, 45:179–194.
<https://doi.org/10.1159/000156227>
- Rosenberger, A.L., Cooke, S.B., Rimoli, R., Ni, X., and Cardoso, L. 2011. First skull of *Antillothrix bernensis*, an extinct relict monkey from the Dominican Republic. *Proceedings of the Royal Society, B, Biological Sciences*, 278:67–74.
<https://doi.org/10.1098/rspb.2010.1249>
- Ross, C.F. 1993. The Functions of the Postorbital Septum and Anthropoid Origins. PhD Thesis, Duke University, Durham, NC.
- Ross, C.F. 1994. The craniofacial evidence for anthropoid and tarsier relationships, p. 469–547. In Fleagle, J.G. and Kay, R.F. (ed.), *Anthropoid Origins: The Fossil Evidence*. Plenum Press, New York.
https://doi.org/10.1007/978-1-4757-9197-6_15
- Ross, C.F. 1995. Allometric and functional influences on primate orbit orientation and the origins of the Anthropoidea. *Journal of Human Evolution*, 29:210–228.
<https://doi.org/10.1006/jhev.1995.1057>
- Ross, C.F., Hall, M.I., and Heesy, C.P. 2007. Were basal primates nocturnal? Evidence from eye and orbit shape, p. In Ravosa, M. and Dagosto, M. (ed.), *Primate Origins: Adaptations and Evolution*. Springer US, New York.
https://doi.org/10.1007/978-0-387-33507-0_7
- Rusconi, C. 1933. Nuevos restos de monos fósiles del Terciario antiguo de la Patagonia. *Anales de la Sociedad Científica Argentina*, 116:286–289.
- Rusconi, C. 1935. Las especies de primates del oligoceno de Patagonia (gen. *Homunculus*). *Revista Argentina de Paleontología y Anthropología Ameghinia*, 1:39–68, 71–100, 103–125.
- Russo, G.A. 2016. Comparative sacral morphology and the reconstructed tail lengths of five extinct primates: *Proconsul heseloni*, *Epipliopithecus vindobonensis*, *Archaeolemur edwardsi*, *Megaladapis grandidieri*, and *Palaeopropithecus kelyus*. *Journal of Human Evolution*, 90:135–162.
<https://doi.org/10.1016/j.jhevol.2015.10.007>
- Saban, R. 1963. Contribution à l'étude de l'os temporal des Primates. Description chez l'Homme et les Prosimiens. *Anatomie comparée et phylogénie. Mémoires du Museum national d'Histoire naturelle (France)*, N. Sér. A, Zool., 29:1–378.

- Sanders, K. 2020. 3D Reconstruction of Fossilized Skull of South American Miocene Monkey *Homunculus patagonicus*: An Augmented Reality for Field Application. MA Thesis, The Johns Hopkins University, Baltimore.
- Seiffert, E.R. 2012. Early primate evolution in Afro-Arabia. *Evolutionary Anthropology*, 21:239-253.
<https://doi.org/10.1002/evan.21335>
- Simons, E.L. 2001. The cranium of *Parapithecus grangeri*, an Egyptian Oligocene anthropoid primate. *Proceedings of the National Academy of Sciences, USA*, 98:7892–7897.
<https://doi.org/10.1073/pnas.051003398>
- Simons, E.L. 2004. The cranium and adaptations of *Parapithecus grangeri* a stem anthropoid from the Fayum Oligocene of Egypt, p. 183–204. In Ross, C. and Kay, R.F. (ed.), *Anthropoid Origins: New Visions*. Kluwer/Plenum Publishing, New York.
https://doi.org/10.1007/978-1-4419-8873-7_8
- Simons, E.L., Seiffert, E.R., Ryan, T.M., and Attia, Y. 2007. A remarkable female cranium of the early Oligocene anthropoid *Aegyptopithecus zeuxis* (Catarrhini, Propliopithecidae). *Proceedings of the National Academy of Sciences of the United States of America*, 104:8731–8736.
<https://doi.org/10.1073/pnas.0703129104>
- Smith, R.J. and Jungers, W.L. 1997. Body mass in comparative primatology. *Journal of Human Evolution*, 32:523–559.
<https://doi.org/10.1006/jhev.1996.0122>
- Stafford, B.P., Rosenberber, A.L., Baker, A.J., Beck, B., Dietz, J.M., and Kleiman, D.G. 1996. Locomotion of Golden Lion Tamarins (*Leontopithecus rosalia*), p. 111–132. In Norconk, M. A., Rosenberber, A.L., and Garber, P. A. (ed.), *Adaptive Radiations of Neotropical Primates*. Plenum Press, New York, NY.
https://doi.org/10.1007/978-1-4419-8770-9_7
- Szalay, F.S. and Dagosto, M. 1980. Locomotor adaptations as reflected on the humerus of Paleogene primates. *Folia Primatologica*, 34:1–45.
<https://doi.org/10.1159/000155946>
- Szalay, F.S. and Delson, E. 1979. *Evolutionary History of the Primates*. Academic Press, New York.
<https://doi.org/10.1016/C2009-0-22035-6>
- Tattersall, I. 1972. The functional significance of airorhynchus in *Megaladapis*. *Folia Primatologica*, 18:20–26.
<https://doi.org/10.1159/000155466>
- Tauber, A.A. 1991. *Homunculus patagonicus* Ameghino, 1891 (Primates, Ceboidea), Mioceno Temprano, de la costa Atlantica austral, Provincia de Santa Cruz, Republica Argentina. *Academia Nacional de Ciencias, Córdoba, Miscelánea*, 82:1–32.
- Tauber, A.A. 1994. Estratigrafía y vertebrados fósiles de la Formación Santa Cruz (Mioceno inferior) en la costa atlántica entre las rías del Coyle y Río Gallegos, Provincia de Santa Cruz, República Argentina. PhD Thesis, Universidad Nacional de Córdoba, República Argentina, Córdoba.
- Tauber, A.A. 1996. Los representantes del género *Protyotherium* (Mammalia, Notoungulata, Interatheriidae) del Mioceno temprano del Sudeste de la Provincia de Santa Cruz, República Argentina. *Academia Nacional de Ciencias de Córdoba*, 95:1–29.
- Tauber, A.A. 1997a. Bioestratigrafía de la formación Santa Cruz (Mioceno inferior) en el extremo sudeste de la Patagonia. *Ameghiniana*, 34:413–426.
- Tauber, A.A. 1997b. Paleología de la formación Santa Cruz (Mioceno inferior) en el extremo sudeste de la Patagonia. *Ameghiniana*, 34:517–529.
- Tauber, A.A. 1999. Los vertebrados de la Formación Santa Cruz (Mioceno Inferior-medio) en el extremo sureste de la Patagonia y su significado paleoecológico. *Revista Española de Paleontología*, 14:173–182.
- Tauber, A.A., Vizcaino, S.F., Kay, R.F., Bargo, M.S., and Luna, C. 2004. Aspectos bioestratigráficos y paleoecológicos de la Formación Santa Cruz (Mioceno temprano-medio) de Patagonia, Argentina. *Ameghiniana*, 41:64.
- Tejedor, M.F., Tauber, A.A., Rosenberger, A.L., Swisher III, C.C., and Palacios, M.E. 2006. New primate genus from the Miocene of Argentina. *Proceedings of the National Academy of Sciences of the USA*, 103:5437–5441.
<https://doi.org/10.1073/pnas.0506126103>

- Tejedor, M. F. and Rosenberger, A.L. 2008. A neotype for *Homunculus patagonicus* Ameghino, 1891, and a new interpretation of the taxon. *PaleoAnthropology*, 2008:68–82.
- Trayler, R.B., Kohn, M.J., Bargo, M.S., Cuitiño, J.I., Kay, R.F., Strömberg, C., and Vizcaíno, S.F. 2020a. Patagonian aridification at the onset of the mid-Miocene Climatic Optimum. *Paleoceanography and Paleoclimatology*, 35, 9:e2020PA003956. <https://doi.org/10.1029/2020PA003956>
- Trayler, R.B., Schmitz, M.D., Cuitiño, J.I., Kohn, M.J., Bargo, M.S., Kay, R.F., Stromberg, C.A.E., and Vizcaíno, S.F. 2020b. An improved approach to age-modeling in deep time: Implications for the Santa Cruz Formation, Argentina. *Bulletin of the Geological Society of America*, 132, 233–244. <https://doi.org/10.1130/B35203.1>
- Vizcaíno, S.F. 2011. Cartas para Florentino desde la Patagonia. Crónica de la correspondencia edita entre los hermanos Ameghino (1887-1902). *Publicación Especial de la Asociación Paleontológica Argentina*, 11:51–67.
- Vizcaíno, S.F., Kay, R.F., and Bargo, M.S. 2012. Background for a paleoecological study of the Santa Cruz Formation (late Early Miocene) on the Atlantic coast of Patagonia, p. 1–22. In Vizcaíno, S.F., Kay, R.F., and Bargo, M.S. (ed.), *Early Miocene Paleobiology in Patagonia: High-Latitude Paleocommunities of the Santa Cruz Formation*. Cambridge University Press, Cambridge. <https://doi.org/10.1017/CBO9780511667381.002>
- Yapuncich, G.S. 2017. Body Mass Prediction from Dental and Postcranial Measurements in Primates and their Nearest Relatives. PhD Thesis, Duke University, Durham, NC.